CCMT

Multi-Fidelity Surrogate-Based Optimization for Exploring the Physics in Explosive Dispersal of Particles

M. Giselle Fernández-Godino

PhD Student (UB-Physics)

UF UNIVERSITY of FLORIDA

NNSA

Departure from Axisymmetry

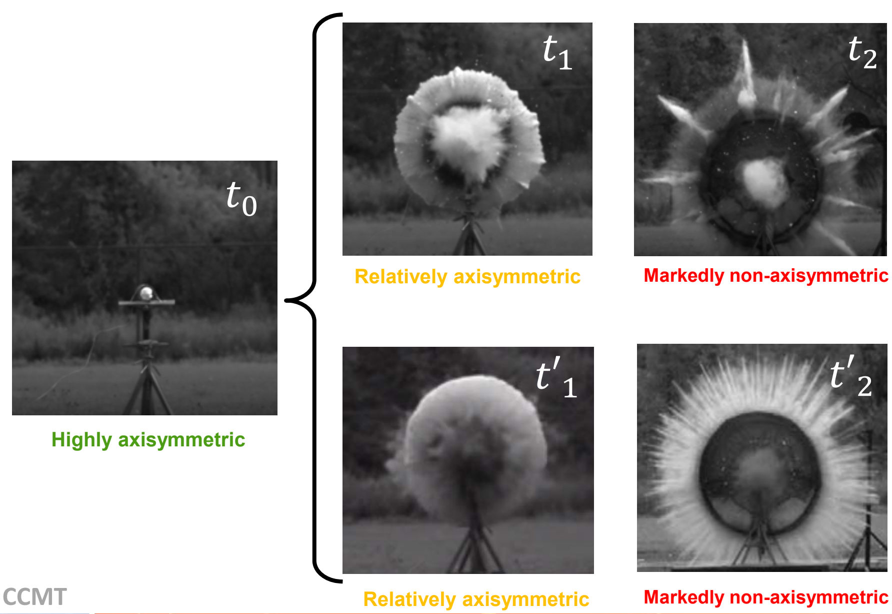

CCMT

2

Questions

- What is a good metric of **departure** from **axisymmetry**?
  - Difference between the volume of particles in the sector with most particles and the one with least

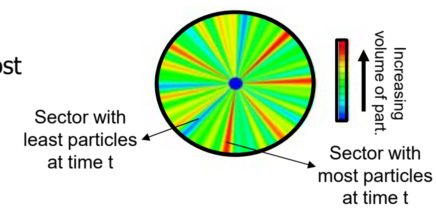

Computational domain

- Which **initial disturbances amplify most** the departure?
  - Multimodal initial PVF perturbations
  - Surrogate models → more than 2,500 simulations already run (9,113,600 core hours)
  - Optimization

CCMT | 3

Parametrization of Initial PVF Perturbation

$$\varphi^p(\theta) = \varphi_o^p[1 + A_1\cos(k_1\theta) + A_2\cos(k_2\theta + \Phi_{12}) + A_3\cos(k_3\theta + \Phi_{13})]$$

φ^p: Particle Volume Fraction (PVF)

φ_o^p: Base PVF

$A_1, k_1, A_2, k_2, \Phi_{12}, A_3, k_3, \Phi_{13}$ → Parameters

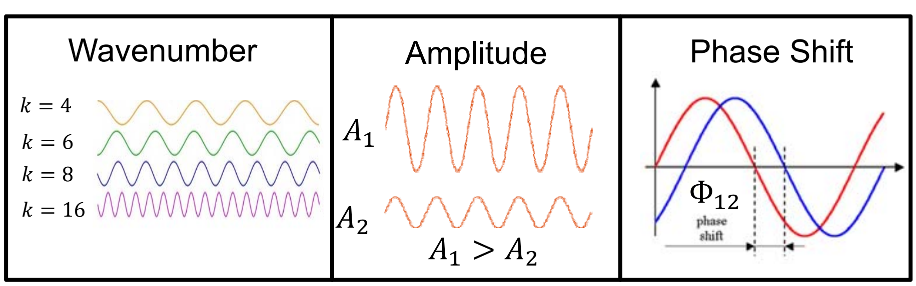

CCMT | 4

Parametrization of Initial PVF Perturbation

$$\varphi^p(\theta) = \varphi_o^p[1 + A_1\cos(k_1\theta) + A_2\cos(k_2\theta + \Phi_{12}) + A_3\cos(k_3\theta + \Phi_{13})]$$

Effective $k = \frac{\sum_{i=1}^{n} k_i}{n}$ Effective $A = \sqrt{\sum_{i=1}^{n} A_i^2} = 0.1\sqrt{2}$

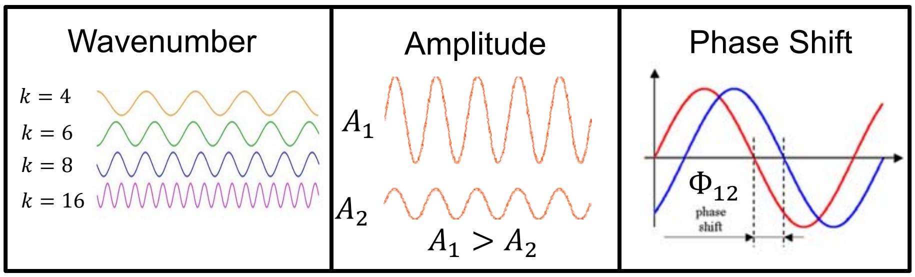

CCMT 5

Illustration from Simulations

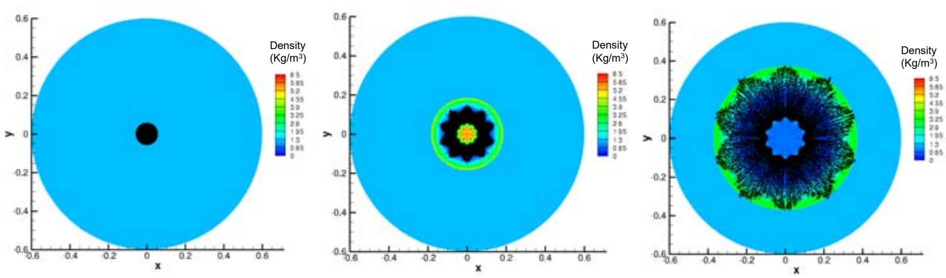

t=0s t=100μs t=300μs

- Computational particles on top of density contours
- Single mode, $k = 10$, $A = 0.1\sqrt{2}$
- Initial sinusoidal angular particle volume fraction (PVF) perturbations translate in finger like structures at later times
- Particles travel faster in sectors where PVF is initially lower

CCMT 6

Amplification of Departure from Axisymmetry

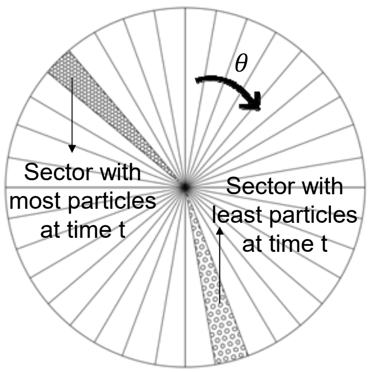

Computational domain is divided in as many sectors as cells in θ

The amplification factor **ζ** is the ratio between the difference of the sector with **most particles** and the one with **least** at time t and the same difference at the initial time t_0

$$\zeta(t) = \frac{Max(f(\theta,t)) - Min(f(\theta,t)}{Max\big(f(\theta,t_0)\big) - Min\big(f(\theta,t_0\,)\big)}$$

where f is the volume of particles in the sector θ at time t

CCMT

7

Amplification factors and volume contours

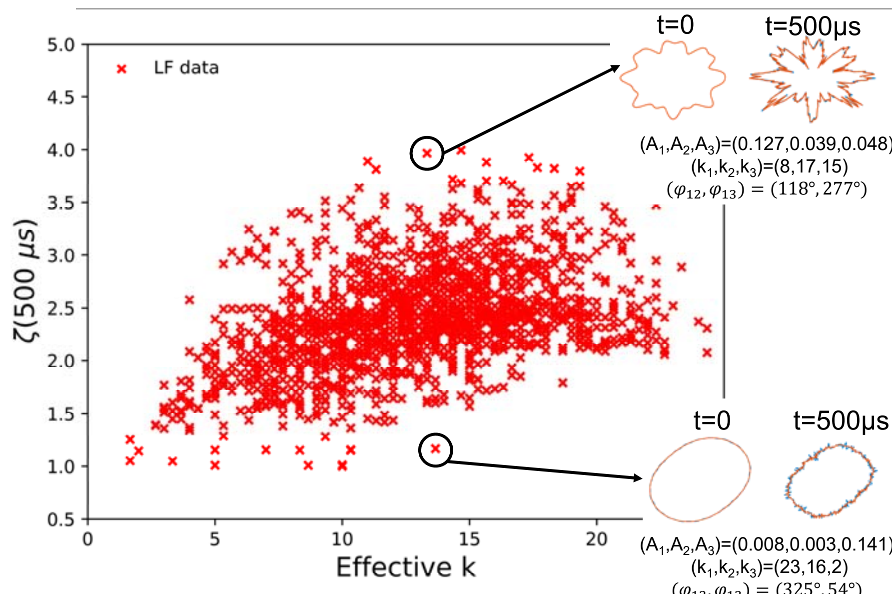

CCMT

8

Amplification factors and volume contours

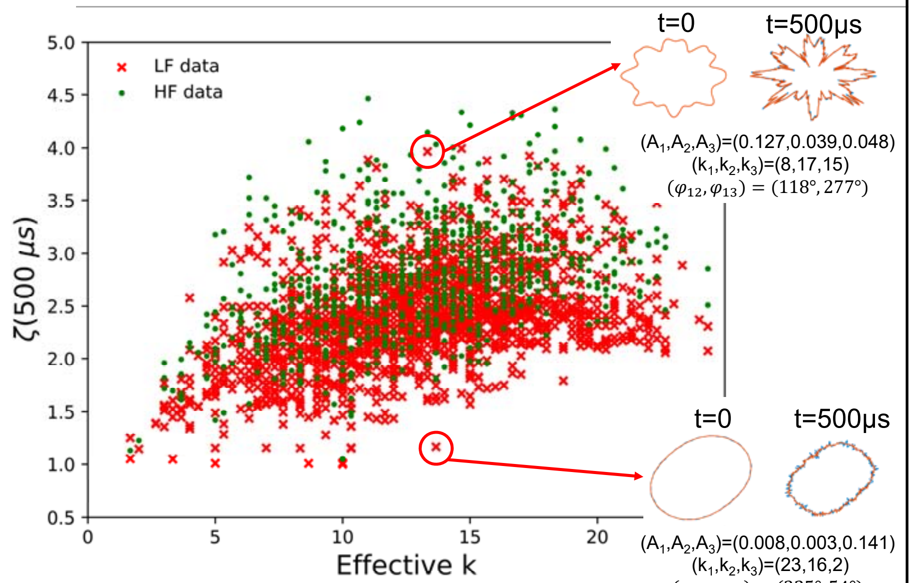

CCMT

9

Surrogate based Optimization

$$\varphi^p(\theta) = \varphi_o^p[1 + A_1 \cos(k_1\theta) + A_2 \cos(k_2\theta + \Phi_{12}) + A_3 \cos(k_3\theta + \Phi_{13})]$$

Parameters

$$\underset{A_1,A_2,A_3,k_1,k_2,k_3,\Phi_{12},\Phi_{13}}{maximize} \quad \zeta$$ } Objective Function

$$Subject\ to\ \sqrt{A_1^2 + A_2^2 + A_3^2} = constant$$ } Energy Constraint

- **LF** (low-fidelity) is a reduced grid of about 0.1HF (high-fidelity) cost
- **MFS** (multi-fidelity surrogate) fits **HF** and **LF** both together
- **Correlation** between LF and HF = 0.9

CCMT

10

Single Parameter Study

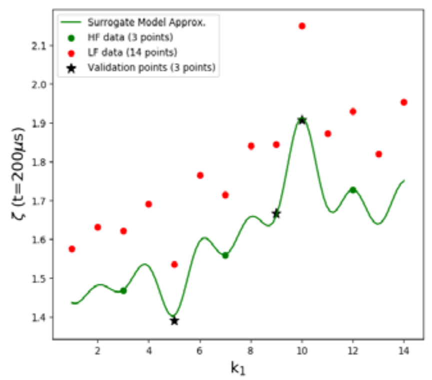

Metric ζ at 200μs as a function of k_1 for HF, LF and Validation points. Continuous green line represents the multi-fidelity model

- **One parameter:** k_1
- Tri-modal perturbation where k_2=15, k_3=25, $A_1=A_2=A_3=\sqrt{2/300}$, $\Phi_{12}=\Phi_{13}=0$ remain constant
- Multi-fidelity surrogate model obtained using **14 LF** points, **3 HF** points and 3 validation points
- The model is able to predict the validation points quite well just with a few HF points
- **General trend:** ζ increases as k increases
- k_1=5 show a lower growth while k_1=10 a higher one. Important triadic interaction between modes!

CCMT

Three-Parameter Study

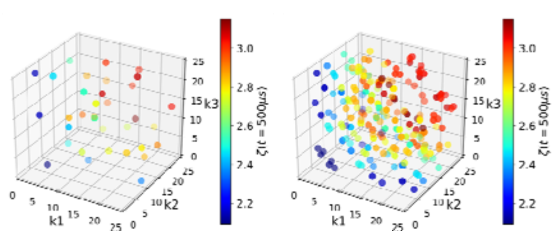

Left. LF data (34 points)
Right. LF data including symmetry points (204=34x6)

CV error	CV error including symmetry points
0.186147	0.042238

- **Three parameters:** k_1 , k_2, and k_3
- $A_1=A_2=A_3=\sqrt{2/300}$, Φ_{12}, Φ_{13}=0 remain constant
- **General trend:** ζ increases as k increases
- Permutations in k does not matter, free symmetry points!
- Bayesian Multi-fidelity surrogate is used
- Symmetry points reduce the cross-validation (CV) error by 77%

CCMT

Conclusions and Future Work

- Initial **2500 runs** show large spread in amplification of departure from axisymmetry
- The future goal is an **optimization** in 7 variables to find the initial disturbance producing a **maximum** amplification of departure from **axisymmetry**
- We have obtained encouraging results using **multi-fidelity surrogate models**. This will allow a reduced cost optimization
- We are finding interesting **interactions between the modes** imposed as a perturbation in the particle volume fraction at the initial time

CCMT

13

CCMT

Do you have any questions?

CCMT

Pairwise Interaction Extended Point-Particle (PIEP) Modeling in nek5000/CMT-nek

W. Chandler Moore

UF UNIVERSITY of FLORIDA

NNSA

Outline

- Context for the PIEP model
- Introduction to the PIEP model
- Effects of the PIEP model on sedimentation tests at low volume fractions
- The use of machine learning to extend the PIEP model to high volume fractions

CCMT | 16

Euler-Lagrange Approach

- Orders of magnitude faster than fully resolved simulations
  - EL & EE only viable approaches for practical problems
  - Point-particle models needed for EL

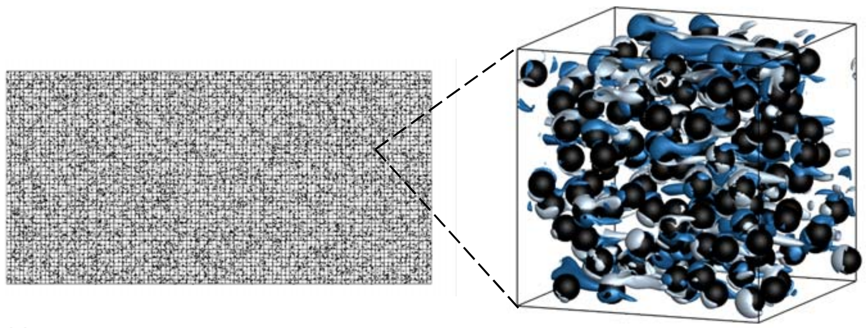

CCMT

17

Governing equations for EL-DEM

Continuous Phase — Incompressible NS equation + feedback force

$$\frac{\partial \boldsymbol{u}}{\partial t} + \boldsymbol{u} \cdot \boldsymbol{\nabla u} = -\boldsymbol{\nabla} P + \frac{1}{Re}\boldsymbol{\nabla}^2 \boldsymbol{u} + \frac{1}{Fr^2}\hat{g} + \boldsymbol{f}_{feedback}$$

Dispersed phase — BBO equation + collision + PIEP

$$m_p \frac{dv}{dt} = (m_p - m_f)g + F_{hydro}(Re, \emptyset) + F_{PIEP} + F_{collision}$$

Collision — Linear elastic + kinematic damping

$$\boldsymbol{F}_{\boldsymbol{pj}}^{\boldsymbol{P}} = \begin{cases} 0 & for\ d_{pj} < (R_{ep} + R_{ej} + \rho), \\ (k_c \delta_{pj} - \eta_c(\boldsymbol{u_p} - \boldsymbol{u_j}) \cdot \boldsymbol{n_{pj}})\boldsymbol{n_{pj}} & for\ d_{pj} < (R_{ep} + R_{ej} + \rho), \end{cases}$$

CCMT

18

Fully Resolved Stationary Simulations

- Immersed boundary method, Grid = $(490)^3$, $d/\Delta x$ = 60

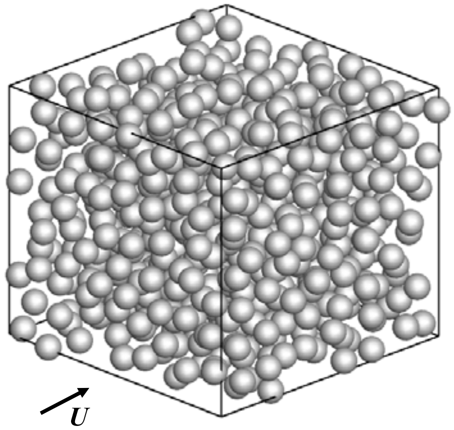

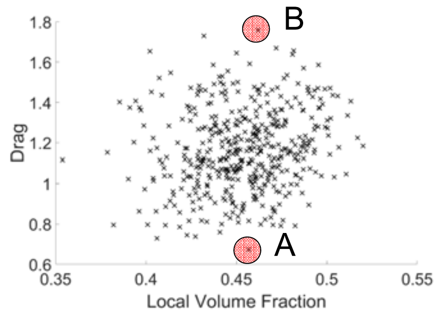

Drag law given by Tenneti et al. (2011)

$\phi = 44\%,\ Re = 20,\ \mathrm{N} = 459$

$$\frac{F_{hydro}}{F_{Sto}} = f(Re,\phi) = \frac{1+0.15Re^{0.687}}{(1-\phi)^3} + \cdots$$

Akiki, Balachandar, JCP, *307*, 34-59 (2016)
Akiki, Jackson, Balachandar, Phys Rev Fluids, 1, 044202 (2016)

CCMT | 19

Pairwise-Interaction Extended Point Particle Model

Drag (stream-wise) Force Map

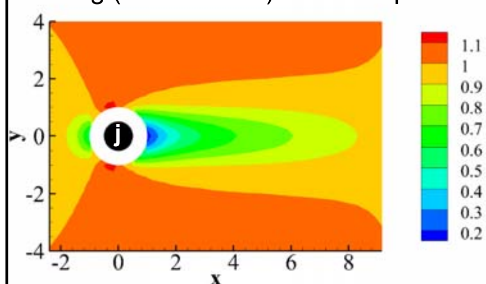

Lift (lateral) Force Map

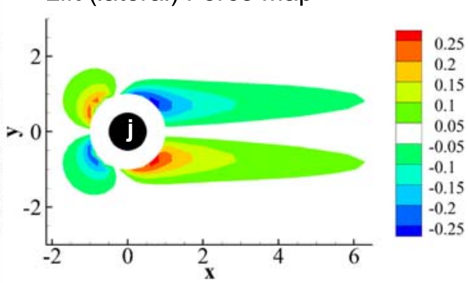

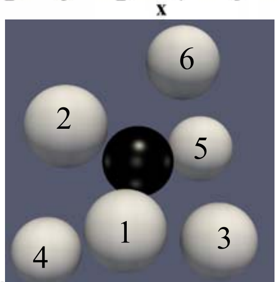

$$F(\boldsymbol{x}_i) \approx \langle F\rangle + \sum_{j=1}^{N} F_{map}(\boldsymbol{x}_i - \boldsymbol{x}_j)$$

Akiki, Jackson, Balachandar, JFM, 813, 882-928 (2017)

CCMT | 20

PIEP model for Drafting, Kissing, & Tumbling

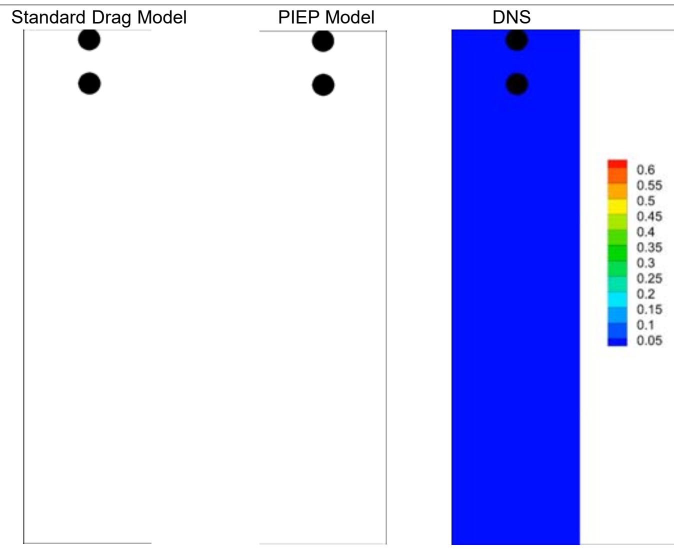

Akiki, Moore, Balachandar, JCP, 351, 329-357 (2017)

CCMT

21

PIEP Model Mesoscale Test

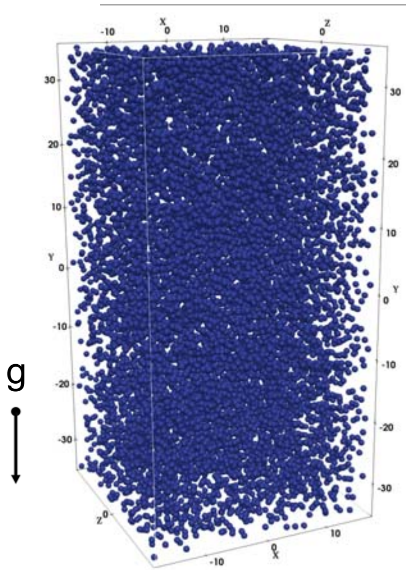

Simulation Settings

- **Geometry**
  - Domain size: $L_x = L_y = 35d$, $L_z = 70d$
  - Average grid width: $\Delta x \cong 0.729$
- **Particle**
  - Total number: $N_p = 11700$
  - Volume fraction: $\emptyset \cong 0.0714$
- **Fluid**
  - Galileo number $\cong 178.46$
  - Two-way coupled
- **Force**
  - Collision, with & w/o PIEP

CCMT

22

UF FLORIDA

PIEP Model Test Results: Collisions

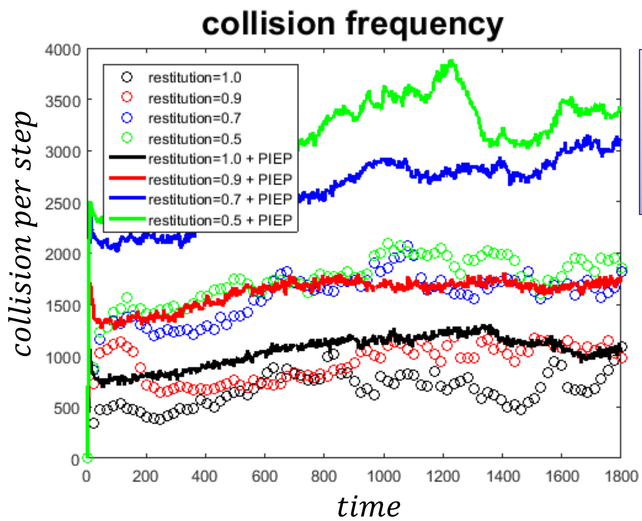

w/o PIEP:
- Lower collision rate

PIEP:
- Intensified collision

CCMT | 23

UF FLORIDA

PIEP Model Test Results: Settling Velocity

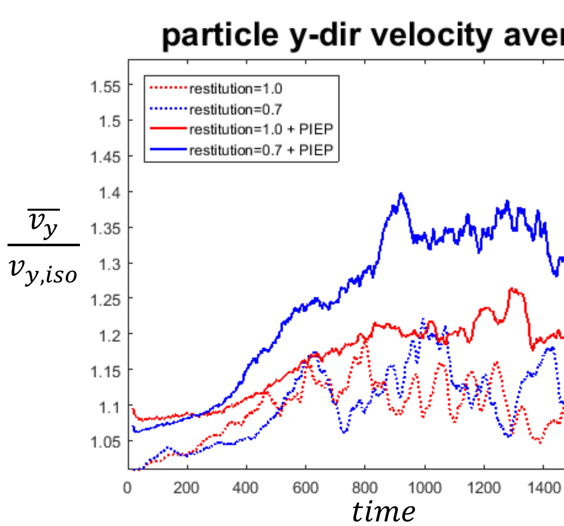

w/o PIEP
- $\overline{v_y}$ Slightly increases
- Not sensitive to restitution

PIEP:
- $\overline{v_y}$ Much larger
- Sensitive to restitution

CCMT | 24

Hybrid Physics-Based Data-Driven Approach

ϕ	*Re*	Realizations
0.1	40, 70, 173	10
0.2	16, 89	8
0.45	20, 115	5

Case	Lift Force R^2 (DNS vs PIEP)
$\phi = 0.1, \quad Re = 40$	0.67
$\phi = 0.2, \quad Re = 16$	0.34
$\phi = 0.45, Re = 20$	0.09

Introducing a data driven $\boldsymbol{F}_{\phi,C}$ term

$$\boldsymbol{F}_{PIEP,Hybrid} = \boldsymbol{F}_{PIEP} + \boldsymbol{F}_{\phi,C}$$

$$\boldsymbol{T}_{PIEP,Hybrid} = \boldsymbol{T}_{PIEP} + \boldsymbol{T}_{\phi,C}$$

where

$$\boldsymbol{F}_{\phi,C} \equiv \boldsymbol{F}_{\phi,C}(Re, \phi, \mathbf{r}_1, \mathbf{r}_2, \ldots, \mathbf{r}_N)$$

$$\boldsymbol{T}_{\phi,C} \equiv \boldsymbol{T}_{\phi,C}(Re, \phi, \mathbf{r}_1, \mathbf{r}_2, \ldots, \mathbf{r}_N)$$

CCMT

Postulated Functional Form

Postulated scaler functions for the drag (*D*), lift (*L*), and torque (*T*) due to a single neighbor:

$$\mathcal{D}_{PIEP-data}(r_x, r_\perp | Re, \phi) = \left(\sum_{m=1}^{M} \sum_{l=0}^{L} \left[\underline{a_{l,m}} j_l(k_{l,m}\, r) + \underline{b_{l,m}} n_l(q_{l,m}\, r) \right] Y_{l,0}(\psi) \right) H(r)$$

$$\mathcal{L}_{PIEP-data}(r_x, r_\perp | Re, \phi) = \left(\sum_{m=1}^{M} \sum_{l=0}^{L} \left[\underline{c_{l,m}} j_l(k_{l,m}\, r) + \underline{d_{l,m}} n_l(q_{l,m}\, r) \right] Y_{l,0}(\psi) \right) H(r)$$

$$\mathcal{T}_{PIEP-data}(r_x, r_\perp | Re, \phi) = \left(\sum_{m=1}^{M} \sum_{l=0}^{L} \left[\underline{e_{l,m}} j_l(k_{l,m}\, r) + \underline{f_{l,m}} n_l(q_{l,m}\, r) \right] Y_{l,0}(\psi) \right) H(r)$$

Where *j* and *n* are the spherical Bessel and Neumann functions and

$$\psi = \tan^{-1}(r_\perp / r_x) \qquad Y_{l,0}(\psi) = \sqrt{\frac{2l+1}{4\pi}} P_l(\cos\psi) \qquad \frac{dj_l(k_{l,m})}{dr} = 0 \quad \text{and} \quad \frac{dn_l(q_{l,m})}{dr} = 0$$

$a_{l,m}$, $b_{l,m}$, …, and $f_{l,m}$ make up the array of parameters to be determined by regression.

CCMT

UF FLORIDA

Coefficient of Determination (R^2) Results

R^2 Values:

		Previous PIEP			Hybrid/Data-Driven PIEP		
ϕ	*Re*	Drag	Lift	Torque	Drag	Lift	Torque
0.1	**40**	0.66	0.67	0.75	0.66	0.73	0.80
0.1	**70**	0.61	0.67	0.65	0.62	0.70	0.72
0.1	**173**	0.33	0.55	0.45	0.43	0.58	0.60
0.2	**16**	0.51	0.34	0.48	0.74	0.75	0.72
0.2	**89**	0.60	0.48	0.72	0.73	0.62	0.78
0.45	**20**	0.12	0.09	0.47	0.64	0.59	0.76
0.45	**115**	0.24	0.19	0.51	0.67	0.57	0.65

$$R^2 = 1 - \frac{\sum_{n=1}^{N_p}\left[F_{DNS}(n) - F_{PI}(n)\right]^2}{\sum_{n=1}^{N_p}\left[F_{DNS}(n) - \langle F_{DNS}\rangle\right]^2}$$

CCMT | 27

UF FLORIDA

Resulting Force Maps (ϕ = 0.45 & *Re* = 20)

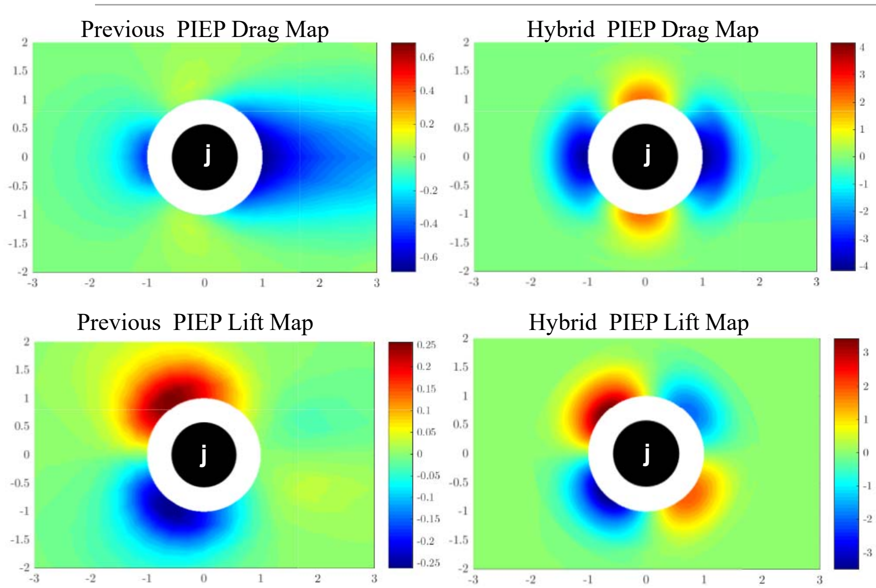

CCMT | 28

UF | UNIVERSITY of FLORIDA

Main Message

- Neighboring particle locations matter
- Previously formulated pairwise interaction extended point-particle (PIEP) model provides accurate forces/torque predictions at low volume fractions
- The implementation of the PIEP model leads to increased collision frequency and settling velocity
- Implementing a data-driven approach allows the PIEP model to predict forces/torques at high volume fractions

CCMT

UF | UNIVERSITY of FLORIDA

Thank you!
Questions?

Acknowledgment:
This material is based upon work supported in part by National Science Foundation Graduate Research Fellowship Program under Grant No. DGE-1315138 and in part by the the U.S. Department of Energy, National Nuclear Security Administration, Advanced Simulation and Computing Program, as a Cooperative Agreement under the Predictive Science Academic Alliance Program, under Contract No. DE-NA0002378.

CCMT

Extra Slides:

CCMT | 31

Exact Location of Neighbors

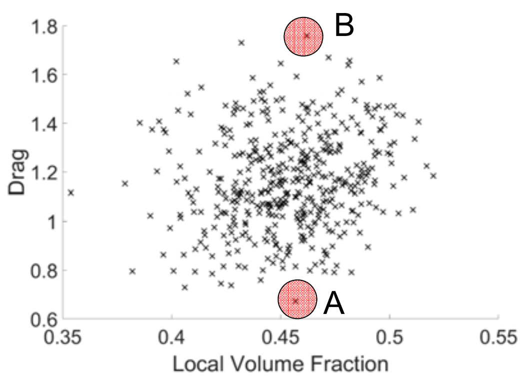

View as seen by Incoming Flow

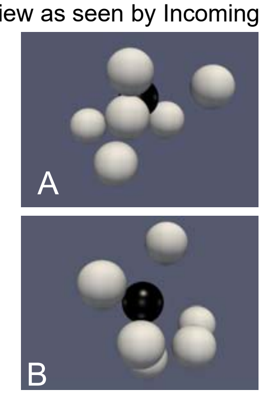

- Local volume fraction cannot explain the variations
- Upstream, downstream, lateral neighbors have different influence

Akiki, Balachandar, JCP, *307*, 34-59 (2016)
Akiki, Jackson, Balachandar, Phys Rev Fluids, 1, 044202 (2016)

CCMT | 32

PIEP Model Test

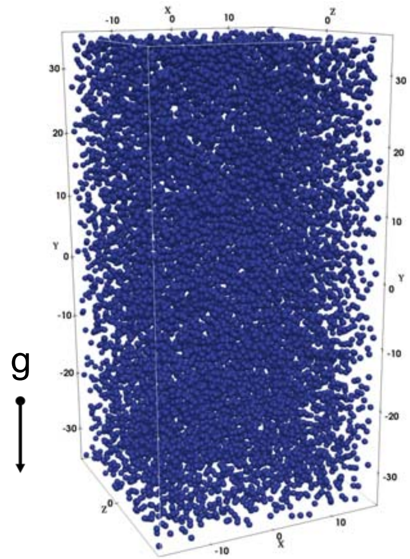

Simulation Settings

- **Geometry**
  - Domain size: $L_x = 35, L_y = 70, L_z = 35$
  - Grid points: $49 \times 97 \times 49 = 232{,}897$
  - Average grid width: $\Delta x \cong 0.729$
- **Particle**
  - Total number: $N_p = 11700$
  - Volume fraction: $\emptyset \cong 0.0714$
- **Fluid**
  - Galileo number $\cong 178.46$
  - Two-way coupled
- **Force**
  - Collision, with & w/o PIEP
- **Other**
  - Uniformly random initial distribution

CCMT

PIEP Model Test Results: Clustering

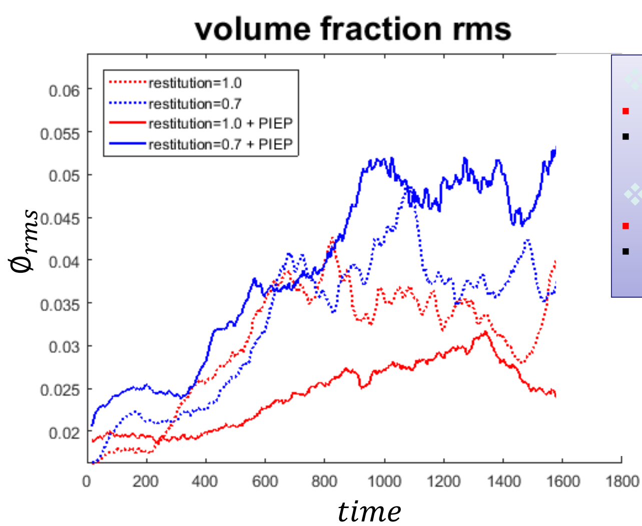

❖ w/o PIEP:
- Weak clustering
- Not sensitive to coefficient of restitution

❖ PIEP:
- Strong clustering
- sensitive to coefficient of restitution

CCMT

PIEP Model Test Results: Other

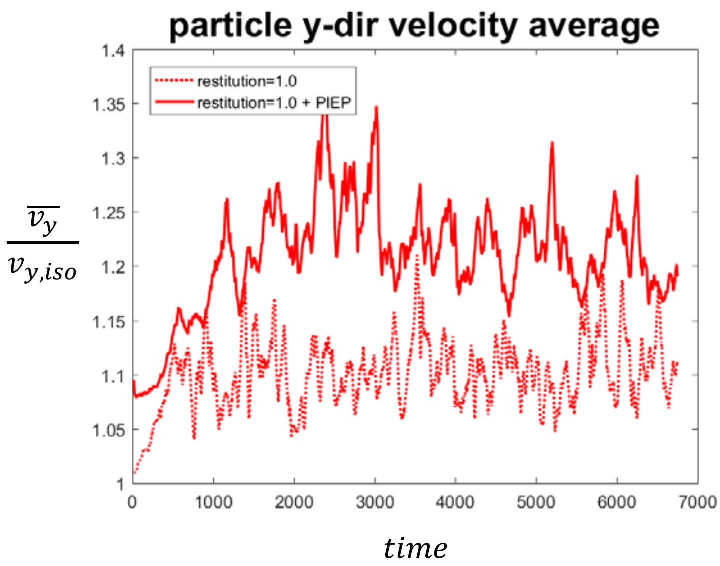

CCMT

35

PIEP Model Test Results: Structure

Restitution = 0.5:

- Volume fraction ($\emptyset =$ 0.20)
- Vertical velocity ($v_y = +1.0$)
- Vertical velocity ($v_y = -1.0$)

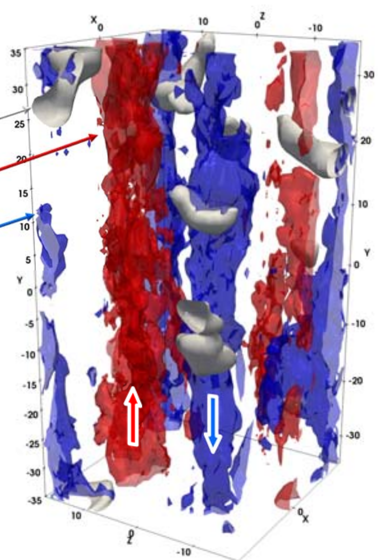

CCMT

36

Current PIEP Model

$$\boldsymbol{F}_{PIEP} = \boldsymbol{F}_{qs} + \boldsymbol{F}_{un} + \boldsymbol{F}_{am} + \boldsymbol{F}_{vu} + \boldsymbol{F}_{L} + \boldsymbol{F}_{c}$$

$$T_{PIEP} = \boldsymbol{T}_{qs} + \boldsymbol{T}_{un} + \boldsymbol{T}_{c}$$

where, using perturbation maps resulting from direct numerical simulations (DNS),

$$\boldsymbol{F}_{PIEP} \equiv \boldsymbol{F}_{PIEP}(Re, \phi, \mathrm{r}_1, \mathrm{r}_2, \ldots, \mathrm{r}_N, \mathrm{v}_1, \mathrm{v}_2, \ldots, \mathrm{v}_N)$$

$$\boldsymbol{T}_{PIEP} \equiv \boldsymbol{T}_{PIEP}(Re, \phi, \mathrm{r}_1, \mathrm{r}_2, \ldots, \mathrm{r}_N, \mathrm{v}_1, \mathrm{v}_2, \ldots, \mathrm{v}_N)$$

CCMT | 37

Regression Modeling (drag)

For a given Re and volume fraction:

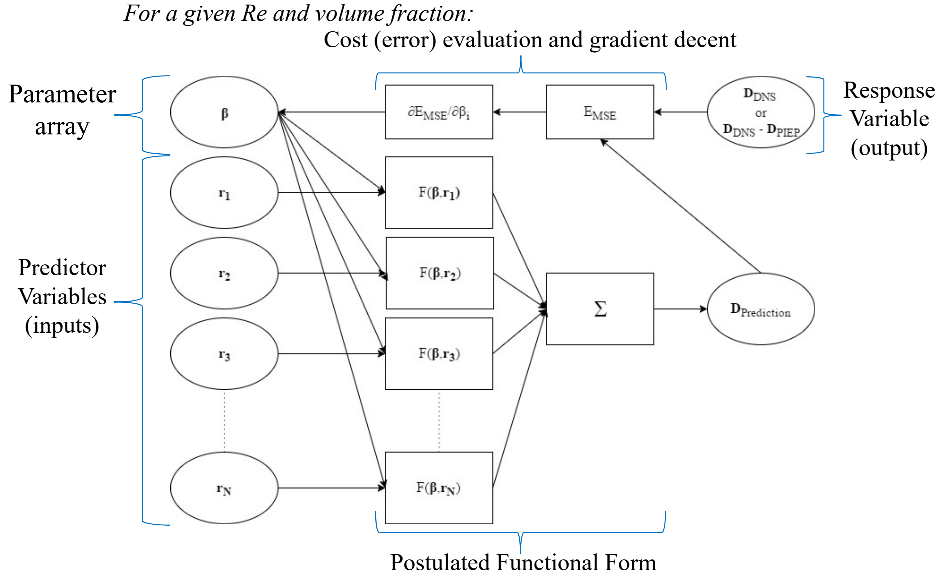

CCMT | 38

Postulating the Functional Form

The function is only defined within radius of influence (r_{max})

$$H(r) = \begin{cases} 0 & r < d \\ 1 & d \leq r \leq r_{max} \\ 0 & r > r_{max} \end{cases}$$

where r_{max} can be found by root finding the following:

$$\int_{V_d}^{V_{r_{max}}} g(r)\rho dV - N_{train} = 0$$

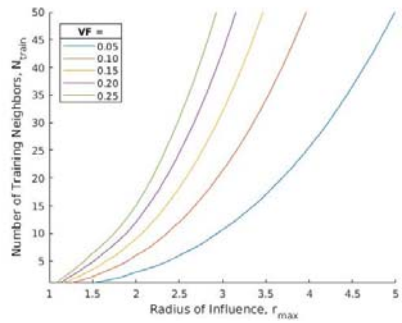

CCMT

CCMT

Fully resolved simulations of expansion waves propagating into particle beds using CMT-nek

Goran Marjanovic

UF UNIVERSITY of FLORIDA

NNSA

Motivation

- Many applications in man-made and natural systems
  - Supernova
  - Blast waves
  - Volcanoes

CCMT

41

Motivation

- Expansion provides a unique contrast between shocked flows (sharp velocity discontinuity) and uniform flows
- Complex physics
  - Compressibility
  - Multiphase flow
  - Turbulence
  - Disparate temporal and spatial scales
- Modeling challenges
  - Validate drag models for meso and macro scale simulations

CCMT

42

Using CMT-nek

Volume Fractions	3%, 10%, 15%
Dimensions	126 x 4 x 4
Elements	29568
Polynomial order	12
DOF	64,960,896
Particle DOF	52,728-210,912
Pressure ratio	4.85
Tail Mach number	0.4
Number of processors	8192 (Mira)

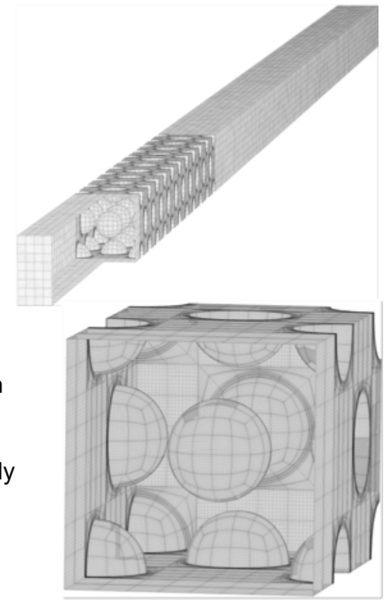

- Frozen particles (porous media)
- Many situations, particles much heavier than gas
  - Particles experience strong force, but acceleration is not very large during early times, so stationary assumption is reasonable
- Inviscid

CCMT

43

Results – 3% Volume fraction

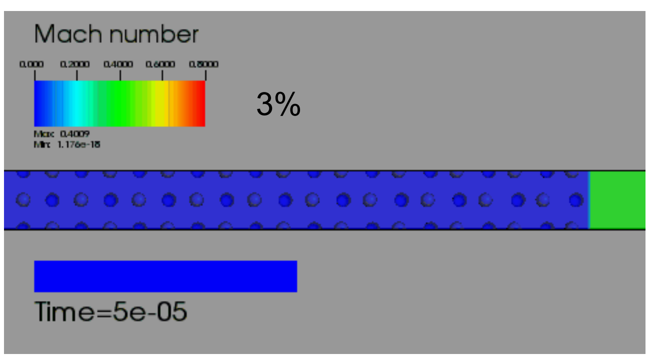

- Between head and tail, sharp change in gradient of velocity
- Velocity of flow passing over particles rapidly increases
- Diffracted/reflected waves propagate upstream
- Post-tail flow particles are subjected to a uniform flow thereafter

CCMT

44

UF FLORIDA

Results – 10%, 15% Volume fraction

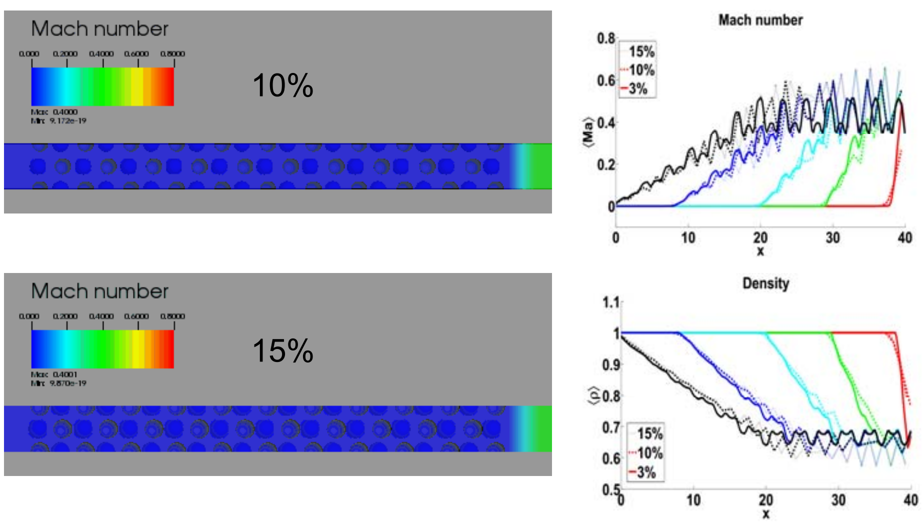

CCMT

45

UF FLORIDA

Results – 3%, 10%, 15% Volume fraction

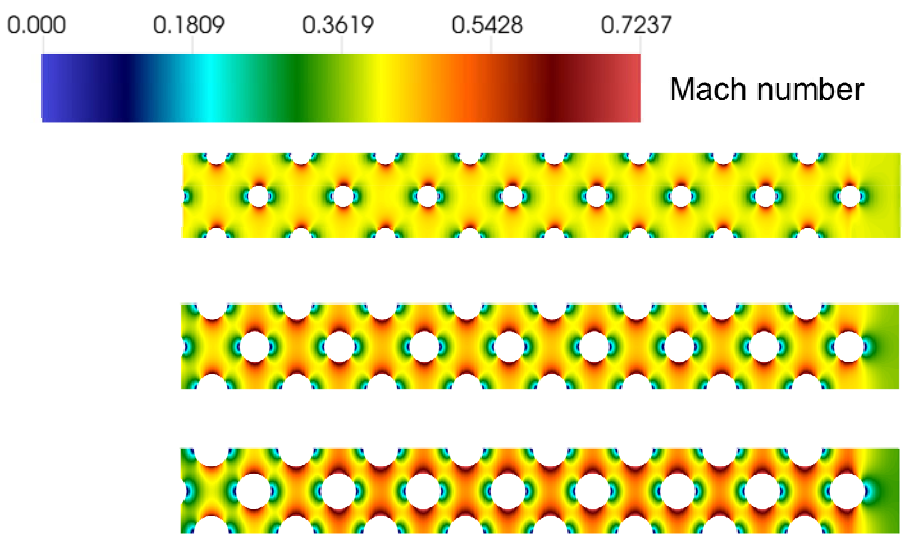

46

UF UNIVERSITY of FLORIDA

Results – Drag model

- Force models (single particle) for compressible flows
- Tested for shock-particle interaction
- Important feature
  - Better able to capture unsteady force effect

(undisturbed/pressure gradient force)

$$\mathbf{F}^{\mathrm{GF}}(t) = \frac{4}{3}\pi R^3 \rho^{\mathrm{un}} \overline{\frac{\mathrm{D}\mathbf{u}^{\mathrm{un}}}{\mathrm{D}t}}^{V} +$$

$$4\pi R^3 \int_{\tilde{\xi}=-\infty}^{\tilde{t}} K_{\mathrm{iu}}(\tilde{t}-\tilde{\xi}; M) \left[\frac{\mathrm{D}}{\mathrm{D}t} \overline{(\rho \mathbf{u}_r)^{\mathrm{un}}}^{S} \right]_{\tilde{t}=\tilde{\xi}} \mathrm{d}\tilde{\xi}$$

(added mass/inviscid unsteady force)

* Annamalai, Subramanian, and S. Balachandar. "Faxén form of time-domain force on a sphere in unsteady spatially varying viscous compressible flows." *Journal of Fluid Mechanics* 816 (2017): 381-411.

CCMT

47

UF UNIVERSITY of FLORIDA

Results – 15% Volume fraction

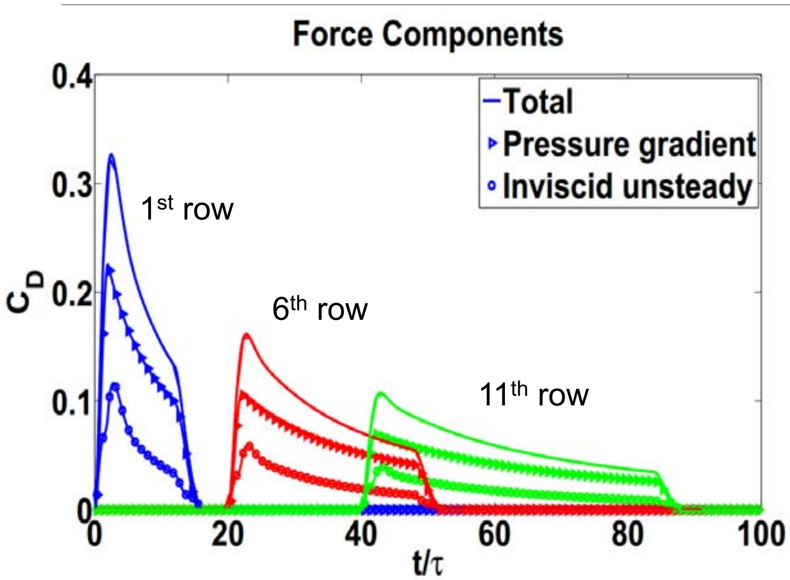

CCMT

48

Results – 3% Volume fraction

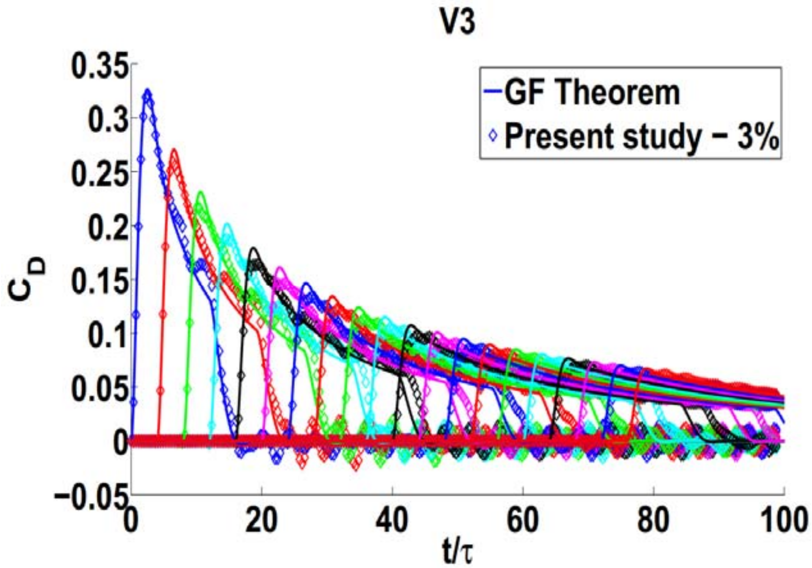

CCMT

49

Results – 10% Volume fraction

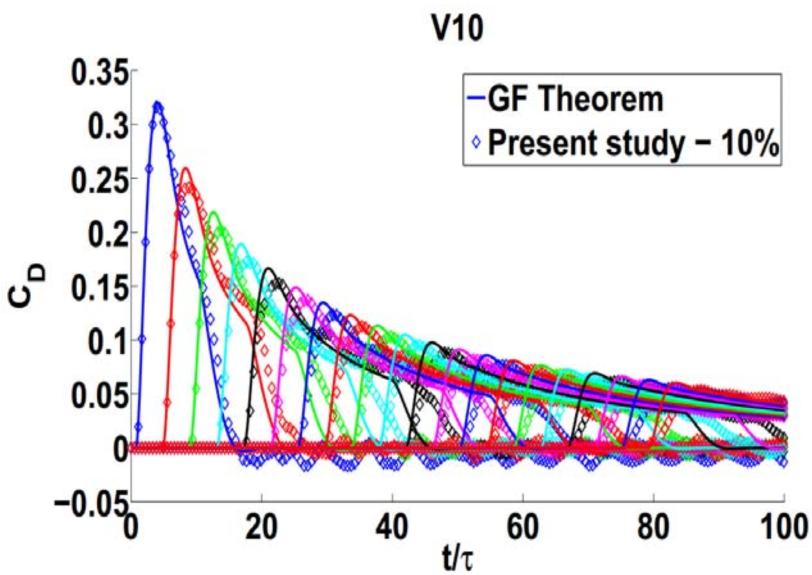

CCMT

50

Results – 15% Volume fraction

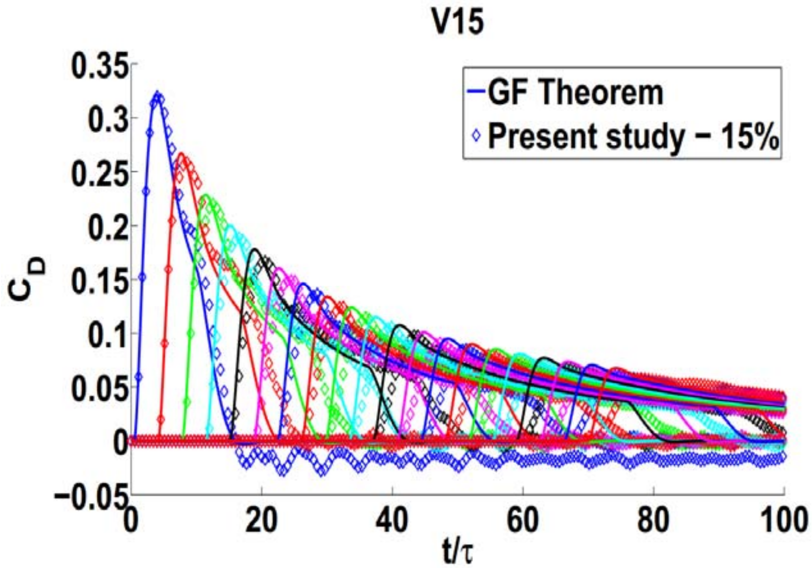

CCMT 51

Nozzle Flow Model

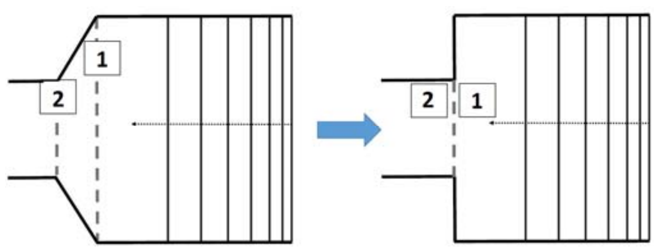

$$\frac{A}{A^*} = \frac{1}{Ma}\left[\left(\frac{2}{\gamma+1}\right)\left(1+\frac{\gamma-1}{2}Ma^2\right)\right]^{\frac{\gamma+1}{2(\gamma-1)}} \Rightarrow \frac{A_2}{A^*} = \frac{A_2}{A_1}\frac{A_1}{A^*}$$

$$\frac{P}{P^*} = \left[\left(\frac{2}{\gamma+1}\right)\left(1+\frac{\gamma-1}{2}Ma^2\right)\right]^{-\frac{\gamma}{\gamma-1}} \Rightarrow P_2 = \frac{P_2}{P^*}\frac{P^*}{P_1}P_1$$

$$\frac{T}{T^*} = \left[\left(\frac{2}{\gamma+1}\right)\left(1+\frac{\gamma-1}{2}Ma^2\right)\right]^{-1} \Rightarrow T_2 = \frac{T_2}{T^*}\frac{T^*}{T_1}T_1$$

CCMT 52

Results – 3%, 10%, 15% Volume fraction

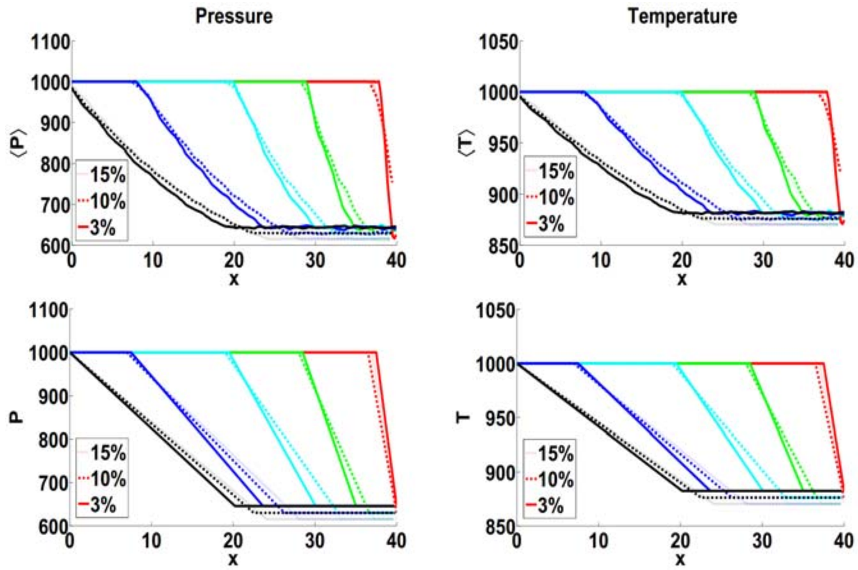

CCMT

53

Conclusions

- Relatively easy to adapt CMT-nek
- Fixed restart capability
- Flow physics
  - Nozzling
  - Acoustic reflections attenuate/modulate drag
- Generalized Faxen's theorem predicts drag relatively well
  - Downstream particles influence upstream
- Unsteady force component contributes significantly at early times
- Inherently complex but fundamentally interesting problem

CCMT

54

UF UNIVERSITY of FLORIDA

Future work

- Explore parameter space
  - Higher Mach numbers
  - Higher volume fractions
- Random arrangement of particles

CCMT

55

CCMT

Do you have any questions?

UF UNIVERSITY of FLORIDA

NNSA

CCMT

Macroscale Explosive Dispersal of Particles at Eglin Blastpad

Kyle Hughes
University of Florida

Angela Diggs and Don Littrell
Eglin Air Force Base, AFRL

UF UNIVERSITY of FLORIDA NNSA

UF UNIVERSITY of FLORIDA

Role in CCMT

Forensic investigation of previous AFRL experiments

Quantify uncertainty in the inputs/outputs

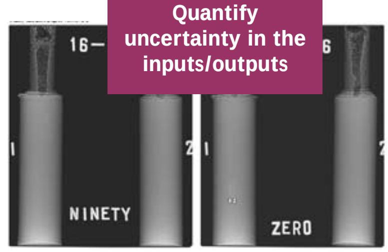

Design of experiments to meet simulation capabilities

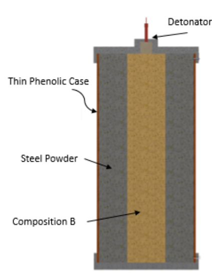

Represent simulations/UQ during testing

CCMT

58

Interaction in Experiment Design

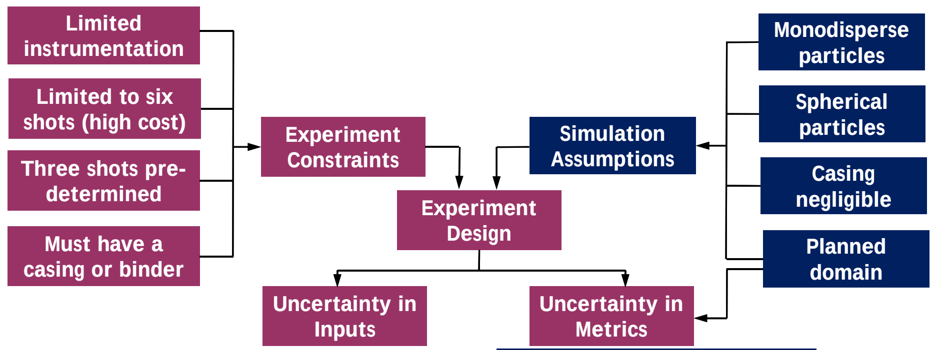

Parameter	Quantity	Method
Explosive Length	44.75 ± 0.08 cm	Tape Measure
Explosive Diameter	8.194 ± 0.008 cm	Caliper
Explosive Mass	4100 ± 24 g	Mass Balance
Particle Diameter	TBD	SEM Image Analysis
Particle Density	7.66 ± 0.03 g/cm^3	Pycnometer
Particle Volume Fraction	TBD	CT Scanner
Ambient Pressure	101.8 ± 0.8 kPa	Eglin Weather Station
Ambient Temperature	32 ± 7 °C	Eglin Weather Station
Probe Locations	± 1%	Tape Measure

Shock location
Particle front location
Peak pressure
Instability number/amplitude

Uncertainty Reduction: Redundant Instrumentation

- Eglin Blastpad chosen as the test site due to additional camera views and large number of pressure transducers (Barreto et al. 2015 contains additional details of the test pad)
- Instrumentation suite consisting of 54 in-ground pressure transducers (sampled at 1 MHz), 6 optical linear encoders, 8 unconfined momentum traps, and 4 high-speed cameras
- Phantom v1212 sampled at 12000 fps (Camera 1/4) and Phantom v711 sampled at 7500 fps

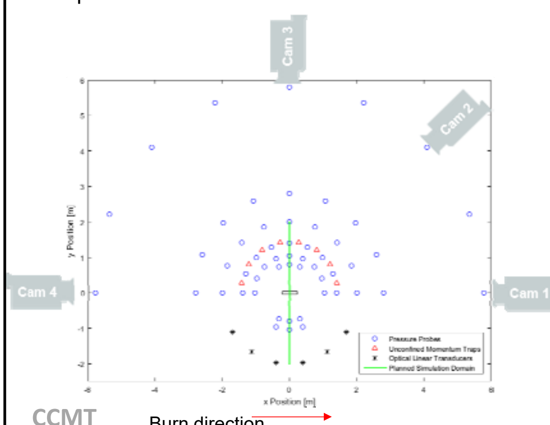

Uncertainty Reduction: Increase Sample Size

- The ratio of the mass of the particles to the mass of the charge (M/C ratio) is critical to formation of instabilities
- Literature review (Frost, Zhang) suggests M/C ≥ 10 is reasonable
- Bare charge geometry is chosen to match legacy blastpad data (increases sample size by two for validation of explosive modeling)

Dimensions in cm

a) Bare charge (Mass = 4.1 kg)

b) Charge w/ tungsten particles (M/C = 10)

c) Charge w/ steel particles (M/C = 13)

CCMT | 61

Uncertainty Reduction: Particle Selection

- Particles chosen to closely match monodisperse and spherical assumptions of the simulations
- Steel Particles
  - Multiple vendors surveyed. Criteria were high particle roundness (sphericity) and narrow particle spread
  - Chosen vendor: Osprey Sandvik
  - Size range (confirmed with particle sizer): 75-125 μm
  - SEM shows mostly spherical particles
- Tungsten Particles
  - Eglin provided
  - Manufactured by Global Tungsten (M70)
  - Size range: 15-40 μm
  - SEM shows angular, irregular particles

SEM of steel particles at 100x zoom.

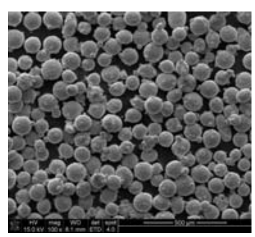

SEM of single steel particle at 1000x zoom.

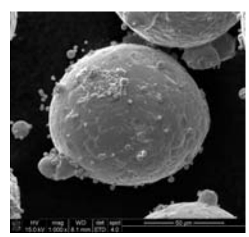

SEM of single tungsten particle, 500x zoom.

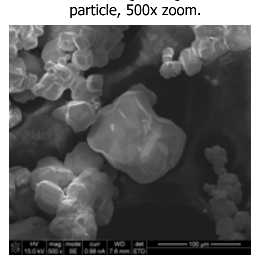

CCMT | 62

UF UNIVERSITY of FLORIDA

Uncertainty Reduction: Negligible Casing

- Case fracture may be a possible mechanism for jetting instability [Zhang et al. 2001, Xu et al. 2013]
- Case influence was minimized by using thin phenolic tubing with no inner casing or struts
- Notches used to attempt to control the failure mechanism in some of the tests

Shot	Liner	Notched?
1	-	-
2	-	-
3	Tungsten	Y
4	Steel	Y
5	Steel	Y
6	Steel	N

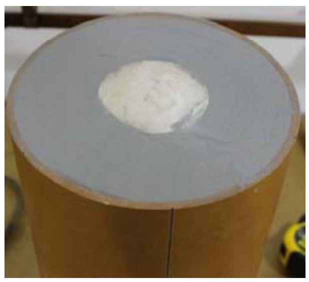

a) Top view of notched casing (steel liner)

b) Casing with steel particle liner aligned with test plane

CCMT

UF UNIVERSITY of FLORIDA

0-Degree Perspective

FPS: 10,000
Elapsed Time: 5.9 ms

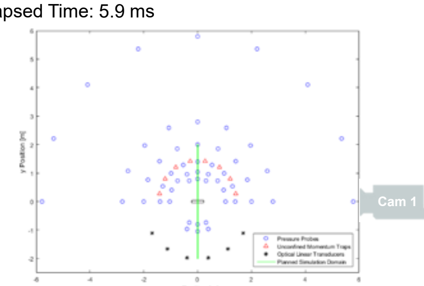

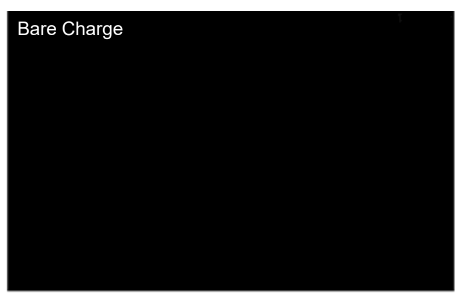

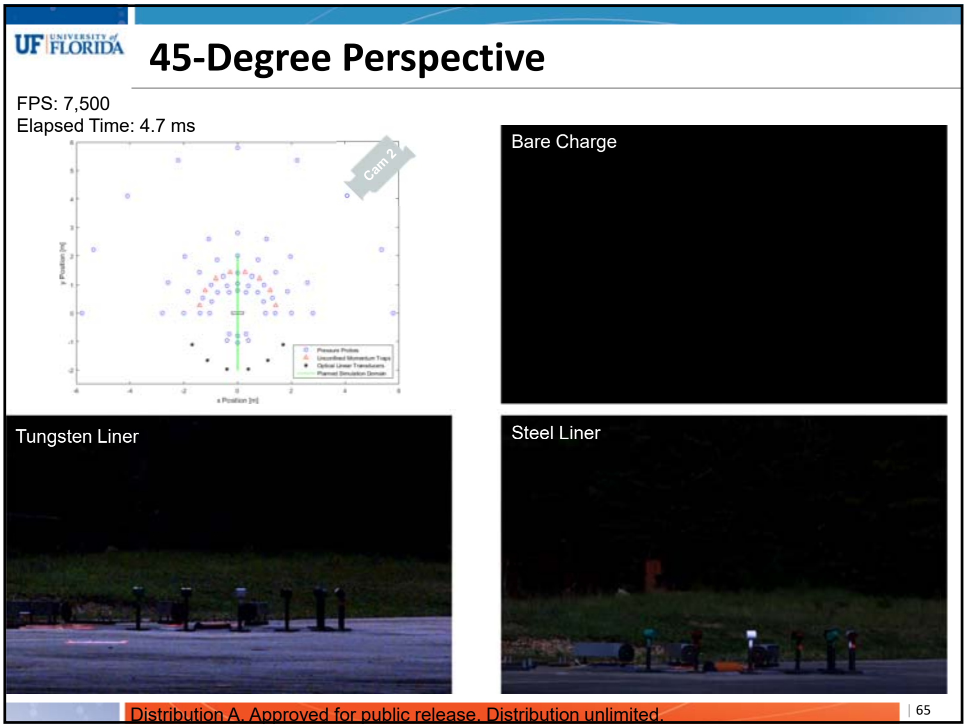
UF UNIVERSITY of FLORIDA
45-Degree Perspective
FPS: 7,500
Elapsed Time: 4.7 ms
Cam 2
Bare Charge
Tungsten Liner
Steel Liner
Distribution A. Approved for public release. Distribution unlimited.
| 65

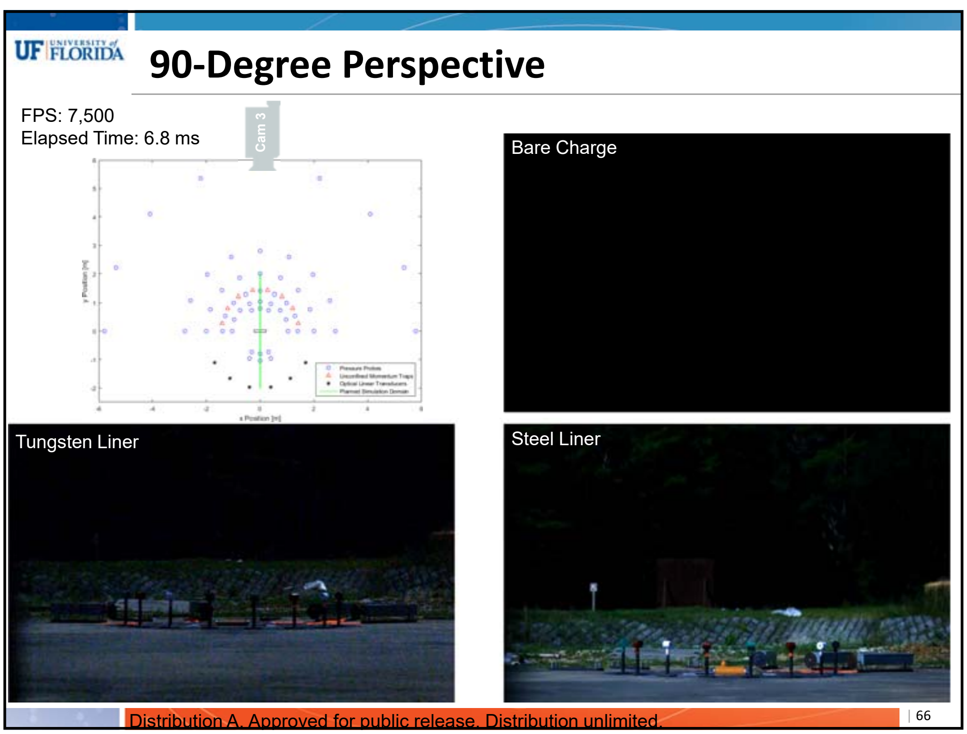
UF UNIVERSITY of FLORIDA
90-Degree Perspective
FPS: 7,500
Elapsed Time: 6.8 ms
Cam 3
Bare Charge
Tungsten Liner
Steel Liner
Distribution A. Approved for public release. Distribution unlimited.
| 66

Test Repeatability: Shock Time of Arrival

Results from 90-degree (centerline) pressure transducers

Tests show highly repeatable shock time of arrival. Casing perturbation does not significantly affect the data.

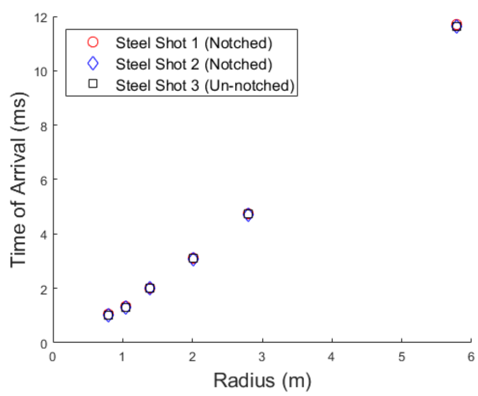

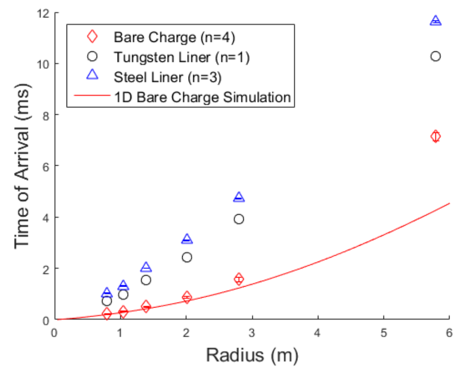

- Results from 90-degree (centerline) pressure transducers
- Vertical error bars = 1σ
- *n* = sample size
- Simulation agrees well at early times and departs at later times

CCMT

Distribution A. Approved for public release. Distribution unlimited.

67

Removal of Perspective Bias

- Shocks analyzed normal to the ground to examine the shock data for ground effects
- Three shock structure forms due to end-cap effect
- To find the shock time of arrival (TOA) along the 90° centerline, camera 3 is used
- Camera 1 and 4 contain significant perspective errors if used to measure shock position on the centerline

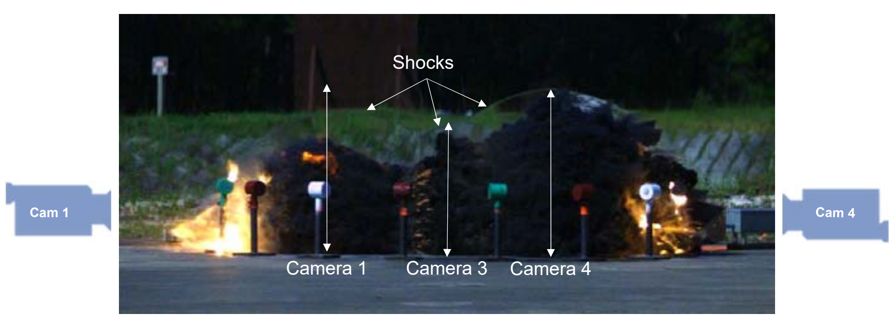

CCMT

Camera 3 at 1.067 ms after detonation showing the differing results for shock position

68

Shock Time of Arrival with Redundant Diagnostics

Redundant diagnostics show data to be in close agreement after removal of bias. No ground effects apparent.

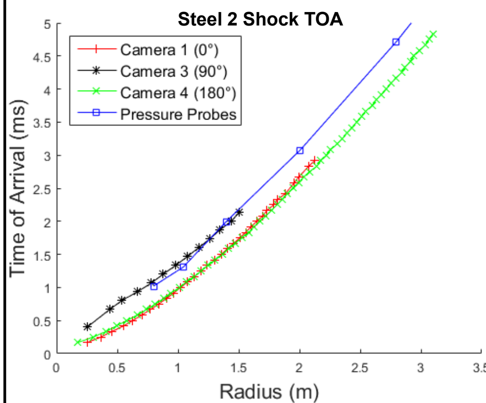

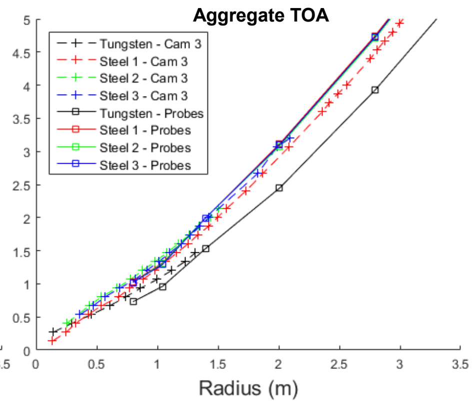

- Camera 1/4 show significant perspective bias compared to camera 3
- High-speed imagery shock time of arrival shows greater variation than the pressure data but greater spatial resolution

CCMT

Distribution A. Approved for public release. Distribution unlimited. 69

LANL Internship – Proton Radiography

60% Initial Vol. Fraction | 40% Initial Vol. Fraction | 20% Initial Vol. Fraction

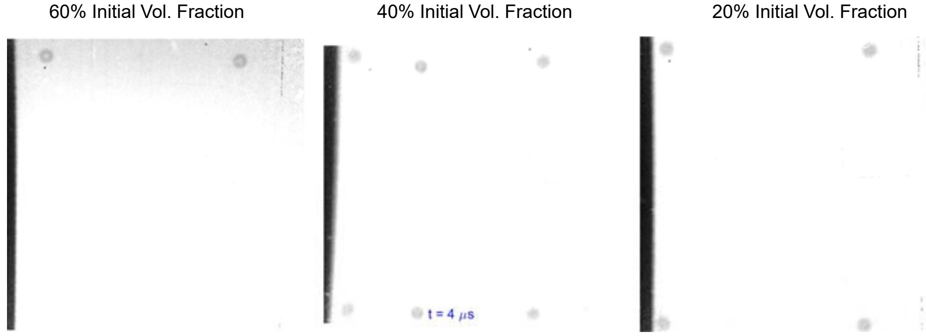

- Further results and discussion during poster session
- Opportunity to perform proton radiography experiments at LANSCE
- Second set of proton radiography experiments proposed for Fall 2018
- **Goal:** Investigate the physics of particle-particle interactions as the bed of particles goes from compaction/collision to dispersal while providing validation-quality data

CCMT

Distribution A. Approved for public release. Distribution unlimited. 70

Conclusions

- Significant collaboration occurred between uncertainty quantification and experimental teams to design the experiment to meet simulation capabilities:
  - Charge designed to take advantage of previous tests
  - Casing influence was minimized through low-strength material and simple design
  - Casing effect was further investigated, and shown to be negligible so far, with small perturbations to casing
  - Particles selected to closely match monodisperse, spherical particle assumptions
- Ongoing measurement and analysis of uncertain inputs for uncertainty propagation through simulations.
- Redundant instrumentation provided multiple measures of shock time of arrival to eliminate sources of uncertainty:
  - Shock tracking data from Cameras 1 and 4 is biased at early times at the centerline
  - Ground effects appear negligible due to agreement between probes and high-speed video
- Validation data provided to multiphase community in a regime where casing is negligible

CCMT | 71

CCMT

Do you have any questions?

CCMT

Experimental Studies of Gas-Particle Mixtures Under Sudden Expansion at ASU

Heather Zunino

PhD Student

Dr. Ronald Adrian

Advisor

UF UNIVERSITY of FLORIDA

NNSA

UF UNIVERSITY of FLORIDA

Problem Statement and Goals

- Experimental multi-phase studies involving compressible flow are complicated
  - Air and solid particles may move separately
  - Particles generate turbulence
- Need for a simple 1D flow experiment that can be used for early validation of the computational codes developed by the PSAAP center.
- Simpler physics involved than the PSAAP capstone experiment
- Perform experiments on existing shock tube setup
- Examine expansion fan, flow structures, turbulence, and instabilities
- Provide data for early-stage validation of computational codes developed by the PSAAP Center

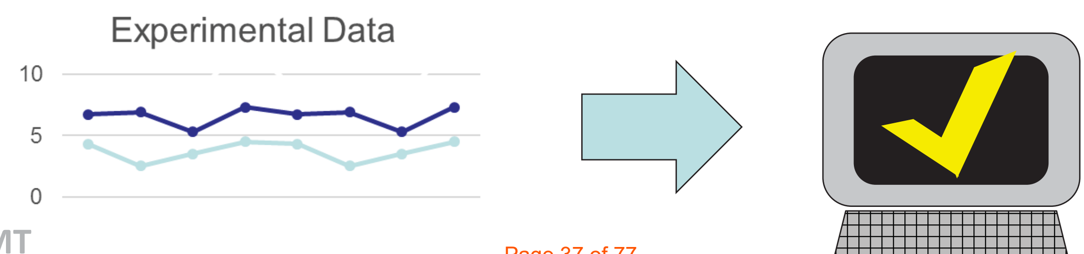

UF | UNIVERSITY of FLORIDA

Experiment Description

- 1 meter glass tube
  - Cylindrical footprint
  - Inner diameter: 3.9cm
- Particle bed
- Diaphragm
  - Tape
- High-speed camera
- Measurements
  - Gas velocity
  - Particle volume concentration
  - Particle interface
- Parameters: particle size, bed height, and pressure ratio

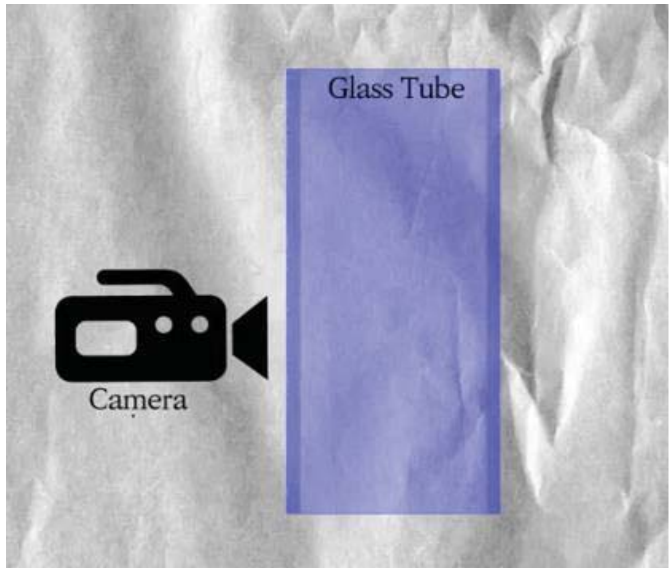

UF | UNIVERSITY of FLORIDA

V&V for the Shocktube Experiment

- 2017 AST Review Comments

1. Complexity of the Experiment
2. Effects of the Sidewalls
3. Identification of the Shock Front
4. Details of Internal Structure

1. Complexity of the Shocktube Experiment

- Diaphragm
  - Rupture
  - Timing
- Bed Packing
  - Controls
  - Simulation
- Measurement Access
  - Particles/field of view
  - PIV seeding
  - Condensation Cloud

Diaphragm

- Begins to melt as soon as current is sent through Nichrome wire
- Usually burns through quickly in a localized section
- The pressure gradient then causes the remaining edges to tear

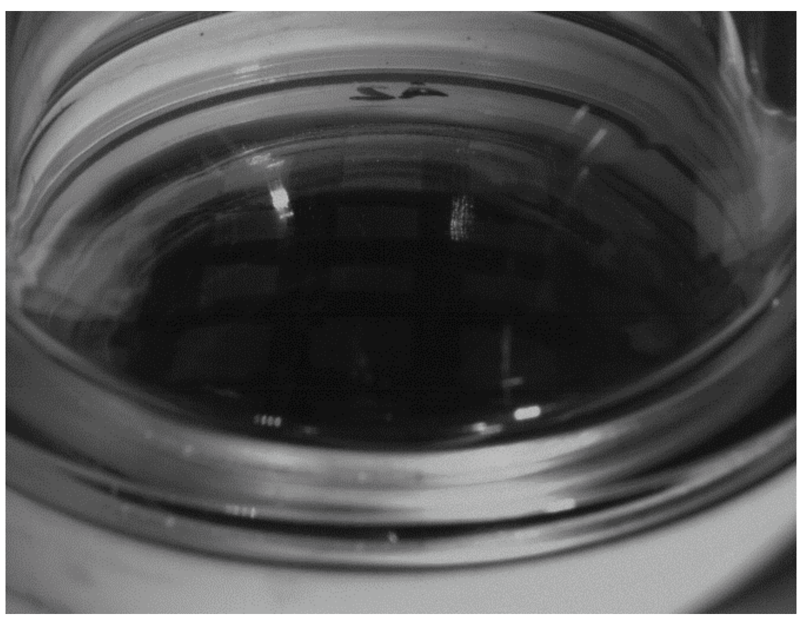

Diaphragm Timings

- Fairly regular

	Realization 1 $P_4/P_1 = 24.03$	Realization 2 $P_4/P_1 = 24.61$	Realization 3 $P_4/P_1 = 21.30$
Duration of large rupture	0.6ms	0.4ms	0.6ms
Duration of expansion	21.19ms	21.75ms	21.42ms
Time between first tear and initial pressure drop	9.255ms	9.165ms	9.165ms
Large rupture event to trigger	0.9ms	0.9ms	0.9ms

Bed Packing

- Polydispersity of bead diameter
- Different pours can result in different overall bed packing density
  - Control for this by measuring mass of particle bed and height every run
  - dV/dm range: 0.0006 to 0.002
- Potential bed packing campaign
  - 3 – 4 different types of pours
  - High-speed video to examine bed unloading
- Initial bed packing simulation
  - B. Vowinckel and E. Meiburg
  - Goal: Investigate irregularities in bed packing that emerge due to the presence of walls after settling under gravity

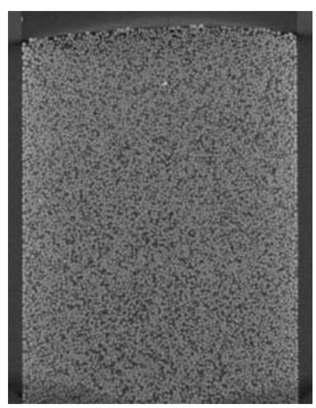
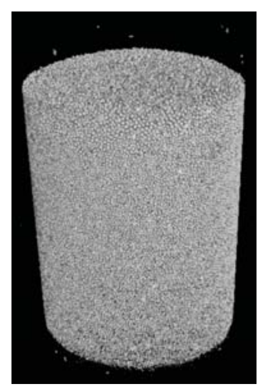
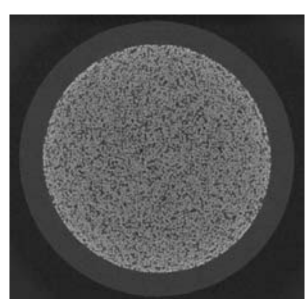

Bed Packing Simulation

- B. Vowinckel and E. Meiburg
- Two infinitely long planes along x-direction
- Separated by 20 particle diameters in z-direction
- 2500 particles and 5000 particles
- 212-297μm
- Wall effect on packing persists for approximately 5 particle diameters

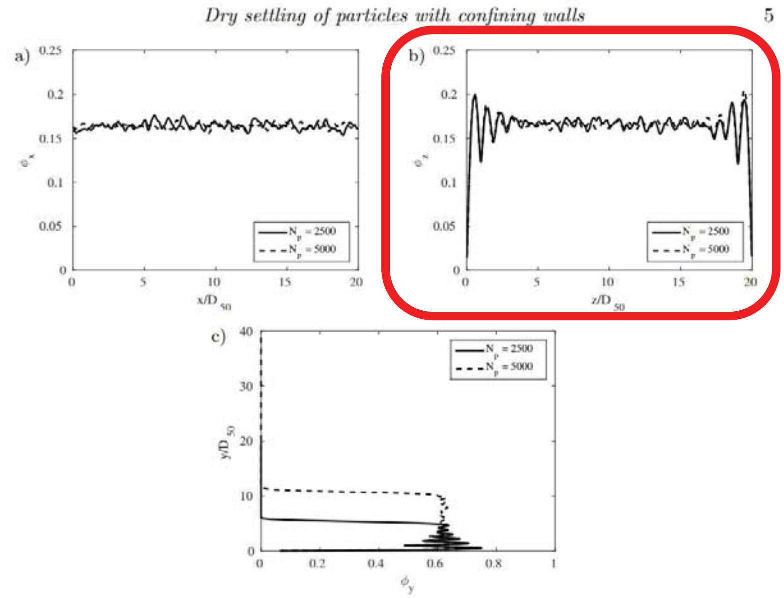

FIGURE 4. *Point-profiles averaged into the different Cartesian directions. (a) averaged in y and z, (b) averaged in x and y, and (c) averaged in x and z.*

Measurement Access

- We have a limited amount of time before the particles take up the entire field of view
- PIV Seeding pushed away from bed
- Cloud can block PIV Data
- Pressure sensor locations

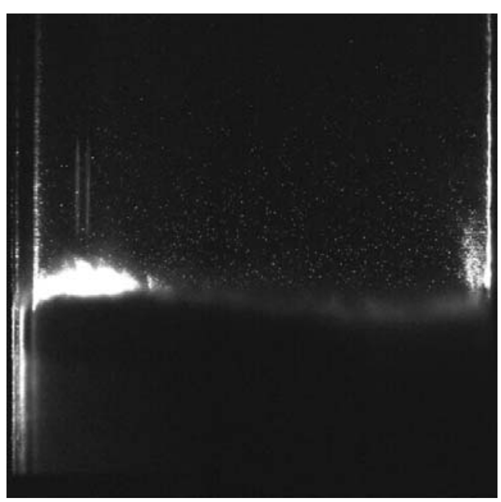

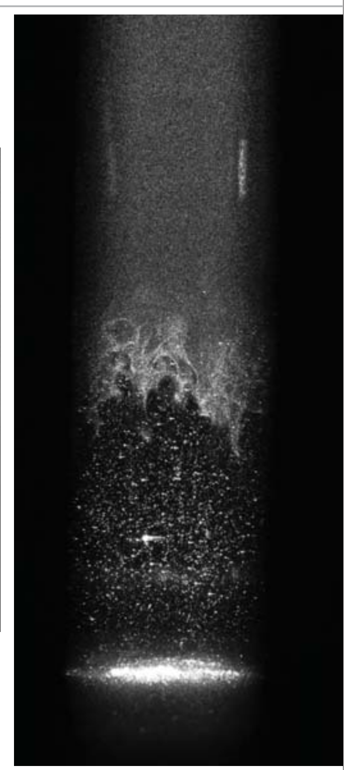

UF UNIVERSITY of FLORIDA

Cloud

- The cloud can block PIV data
- Different bed heights change the pressure drop, as seen by the two pressure sensors 35cm below the diaphragm
- Smaller $z_d - z_0$ yields a faster pressure drop and a faster arrival of the cloud

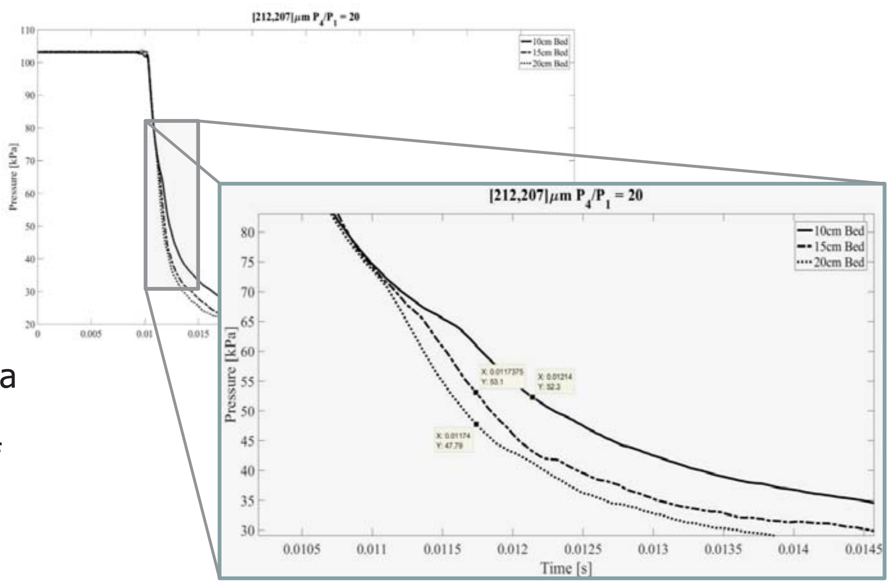

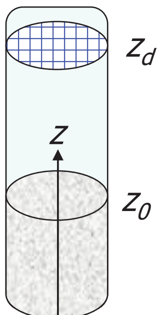

- *Timing for 15cm bed was calculated using PIV, with much higher light intensity and timing resolution

UF UNIVERSITY of FLORIDA

2. Effect of Sidewalls

- Simulation of initial bed packing
  - Bed Packing Discussion
- Perimeter of particle bed interface
  - Near-wall particle motion
  - Cloud recession
- Imperfect joints
  - Very slight roughness
  - Reflected shock

Particle Interface Perimeter

- Bright pixels indicate change from initial image
- Edges of particle bed interface change first
- Δt = 0.0016s

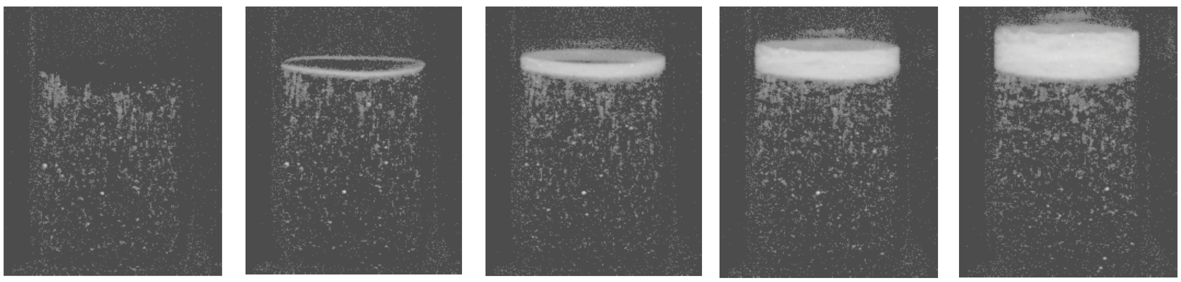

$t = t_0$	$t = t_0 + \Delta t$	$t = t_0 + 2\Delta t$	$t = t_0 + 3\Delta t$	$t = t_0 + 4\Delta t$

Particle Interface Perimeter (cont.)

- The edges of the particle bed interface rise and deform faster than the interior of the interface
- The bed swells briefly and then breaks into cracks/cells
  - Later, the interface deformation begins—starting along the perimeter

- Edge of interface develops wave-like features
  - Approximately 6cm^2 (12.5%) of the interface is deformed

- Sharp structures develop along perimeter of particle bed
  - Approximatel y 16.5cm^2 (35%) of the interface is deformed

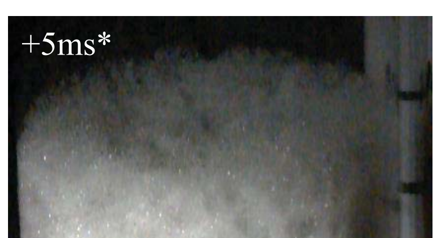

- Sharp structures develop in the center of particle bed
  - Approximately 30cm^2 (62.5%) of the interface is deformed

*times are relative to the first sign of movement at the top of the particle bed

3.7kPa

Cloud Recession and Bed Rise

- The conical shape of the cloud in later frames suggests degassing of the particle bed occurs earlier (or faster) along the perimeter of the bed interface

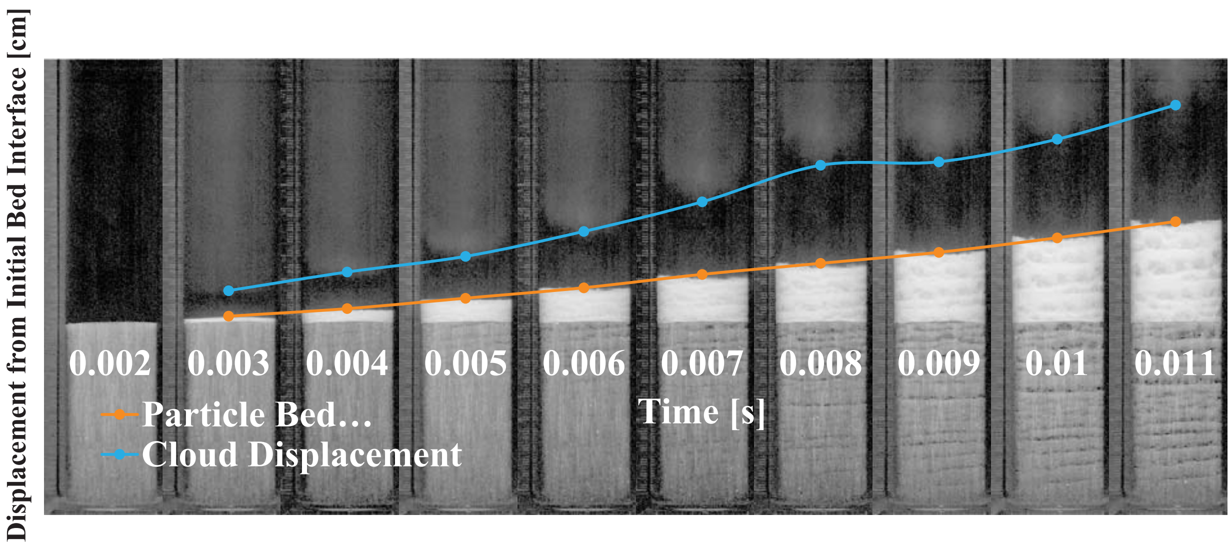

3. Identification of Shock Front

- Triple Pressure Sensor
- Shock Acceleration Campaign
- Shock "quality" highly associated with "quality/regularity" of expansion/bed degassing, as measured by PIV

UF UNIVERSITY of FLORIDA

"Triple Pressure Sensor"

- Three pressure sensors used to capture shock front
- 4 realizations shown
- Ensemble average of all sensors and realizations shown in orange
- All "12" triggered at exactly the same time

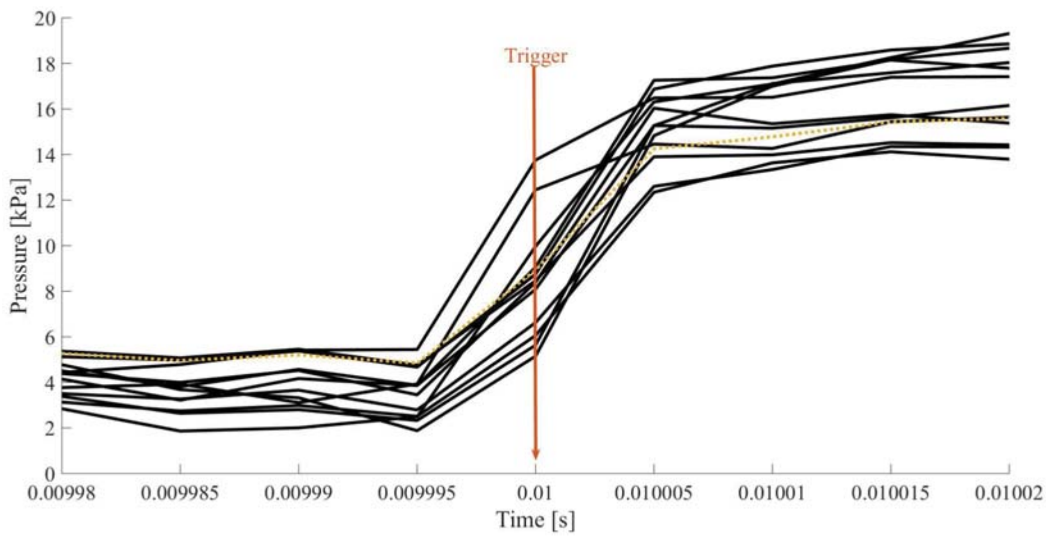

CCMT

UF UNIVERSITY of FLORIDA

Shock Acceleration Campaign

- Measured shock velocities between three locations
- At ~600m/s, we can measure with an uncertainty of +/- 2.5m/s due to our sampling rate
- For three runs, all shock velocities were the same between all three locations

Run	P4 [kPa]	P1 [kPa]	P2	P4/P1	P2/P1	t1 [s]	t2 [s]	Measured Cs [m/s]
022118_2	103.31	4.9	18.2	21.1	3.7	0.010005	0.010585	586.2 Between A I4,5 and AI 1,2,3
			19.7		4.0	0.010585	0.011155	596.5 Between AI 1,2,3 and AI0
022218_1	103.26	4.9	16.2	21.1	3.3	0.009995	0.01057	591.3 Between A I4,5 and AI 1,2,3
			20.2		4.1	0.01057	0.011145	591.3 Between AI 1,2,3 and AI0
022218_2	103.24	4.84	16.3	21.3	3.4	0.009995	0.010575	586.2 Between A I4,5 and AI 1,2,3
			18.5		3.8	0.010575	0.01115	591.3 Between AI 1,2,3 and AI0

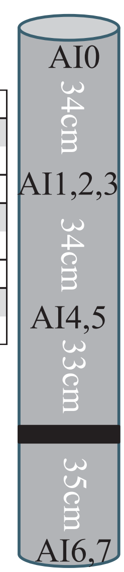

CCMT

Shock "Quality"

- When shock quality is "poor" we can see lower velocities in the PIV Data

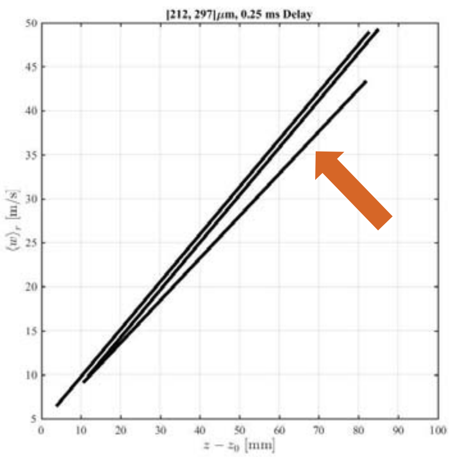

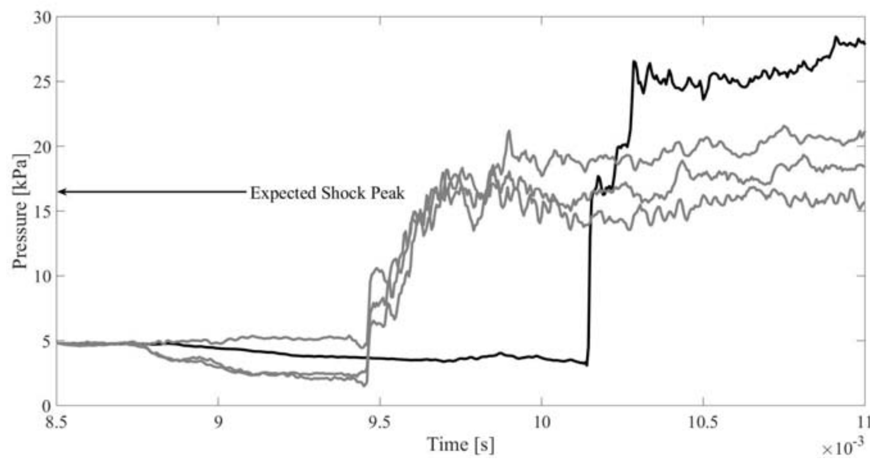

4. Details of Internal Structure

- "Cracks and voids"
- New way to measure external structures
  - Streak Images
  - May provide insight to internal structures
- Shadowgraphy
  - Fiber optic cable along central axis of particle bed
  - Variation in intensity across image
- Possibility of internal structure measurement at Nat'l Lab
  - Flash X-Ray Tomography

UF UNIVERSITY of FLORIDA

Cracks and Voids

- We can see the "backs" of particle vacant regions
- These features visible from the outside do not penetrate all the way through the bed
- There may be similar structures in the interior that are blocked from view

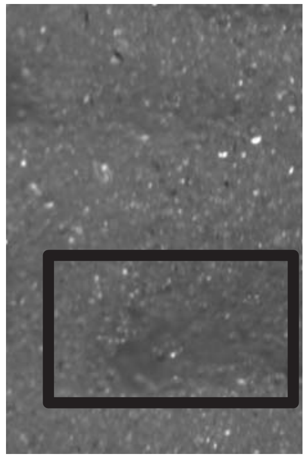

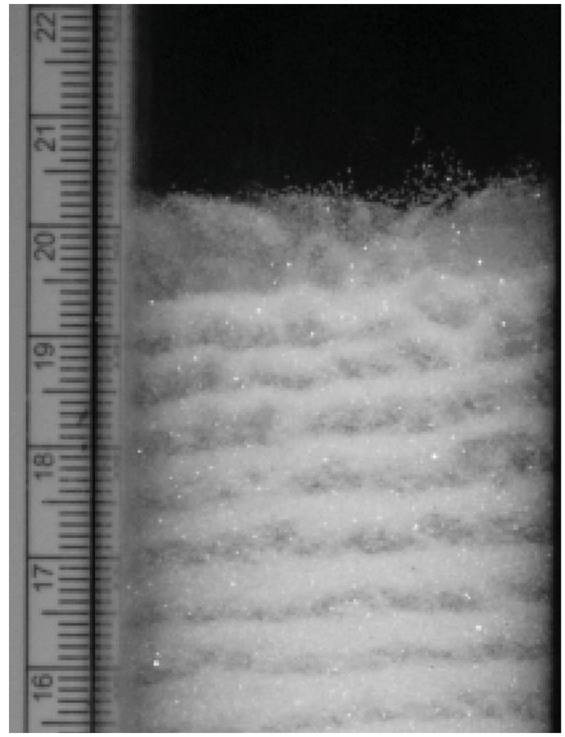

UF UNIVERSITY of FLORIDA

Streak Images

- Width of tube: 6 sections, [212, 297]μm
- Each column is the intensity averaged over 20 pixels
- The x-axis time, system received trigger at t = 0

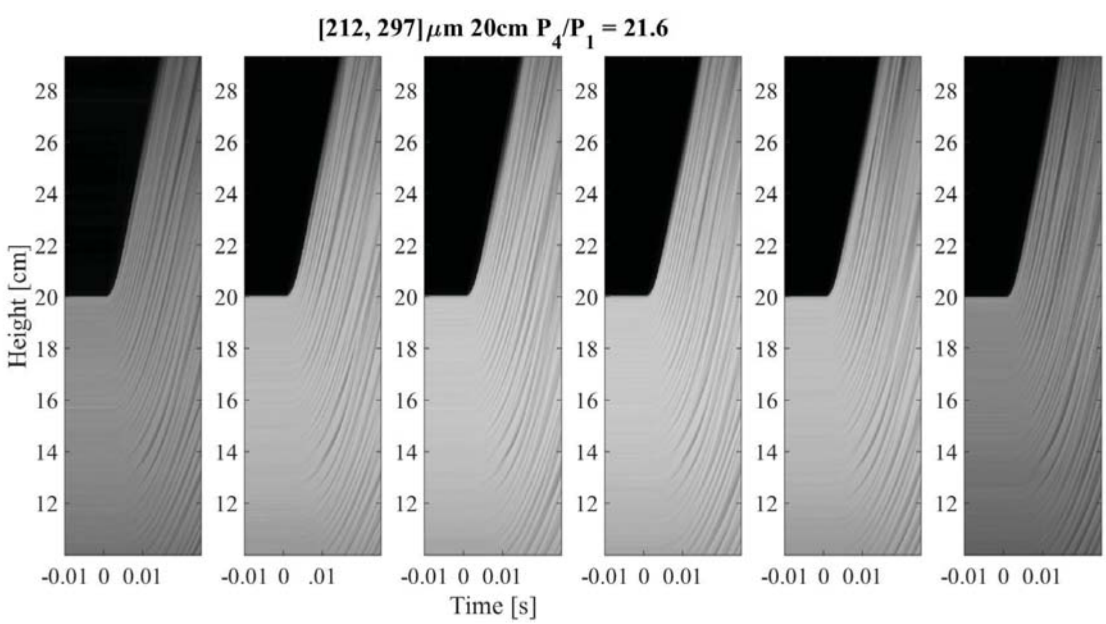

Streak Images

- Width of tube: 6 sections, [44, 90]μm
- Each column is the intensity averaged over 20 pixels
- The x-axis time, system received trigger at t = 0

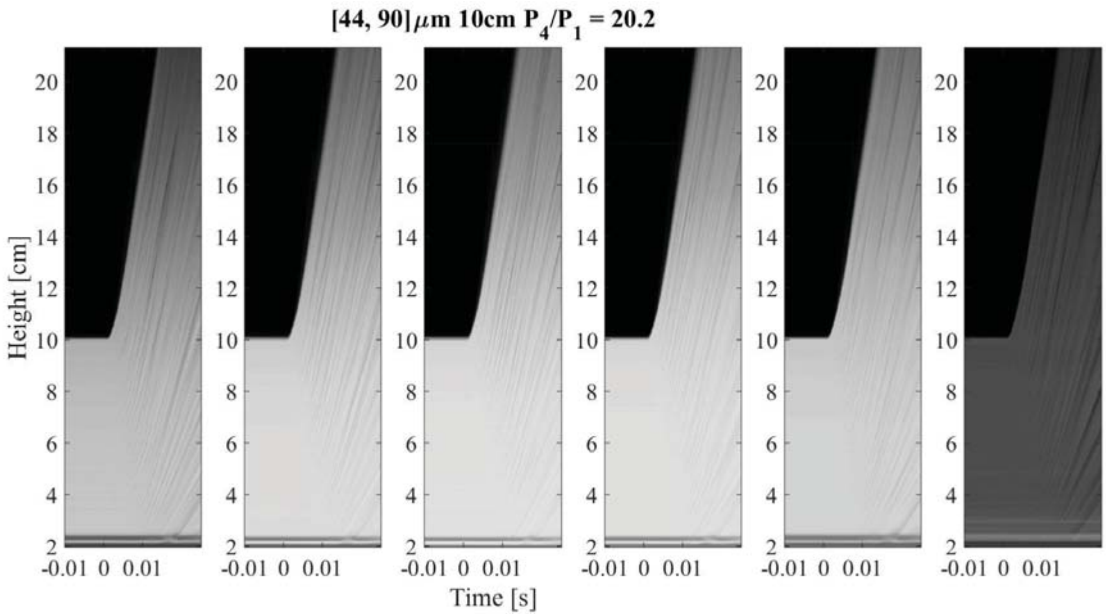

Summary

- Complexity of experiment
  - Reliable diaphragm timing and controls for bed packing
- Effects of the sidewalls
  - Observable, initial wall effect persists for 5 bead diameters
- Identification of the shock front
  - Very reliable identification of shock front
- Details of internal structure
  - Not observable, new methods to measure external structures
  - Potential future experiments

Results

- Effect of particle size and initial bed height on bed displacement
  - Ensemble average of 5 realizations for each experiment

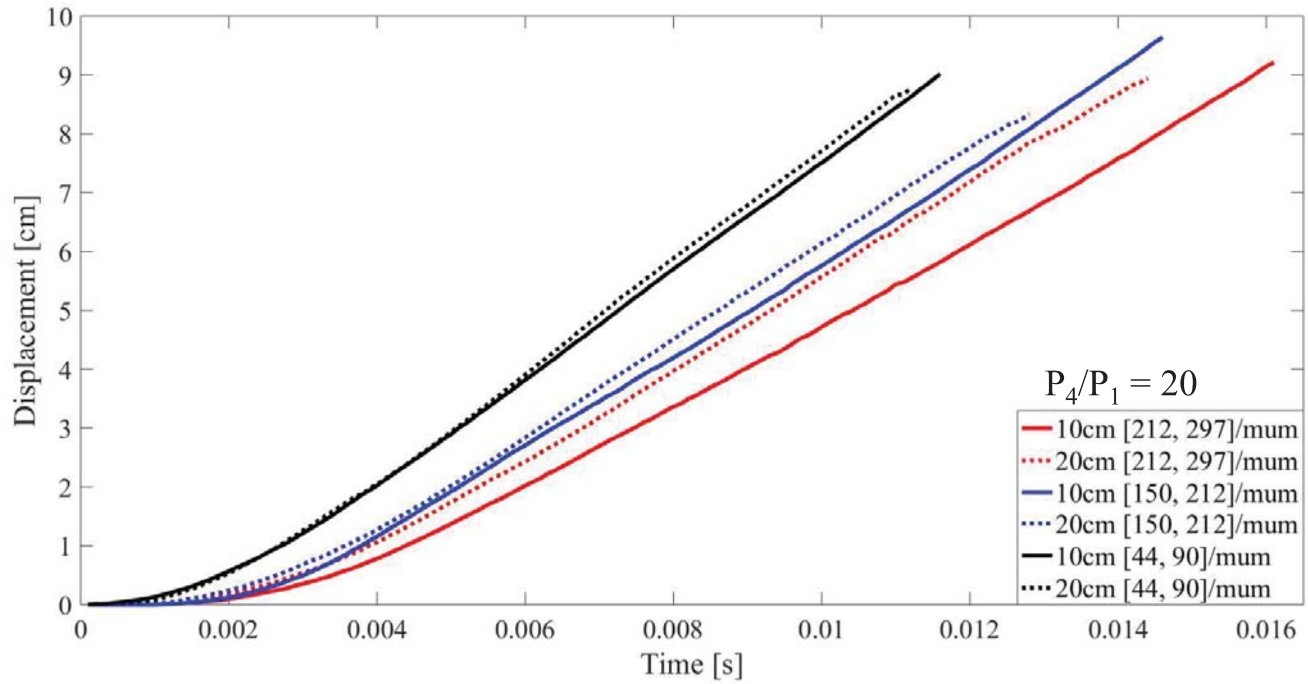

Results

- Effect of particle size and initial bed height on pressure

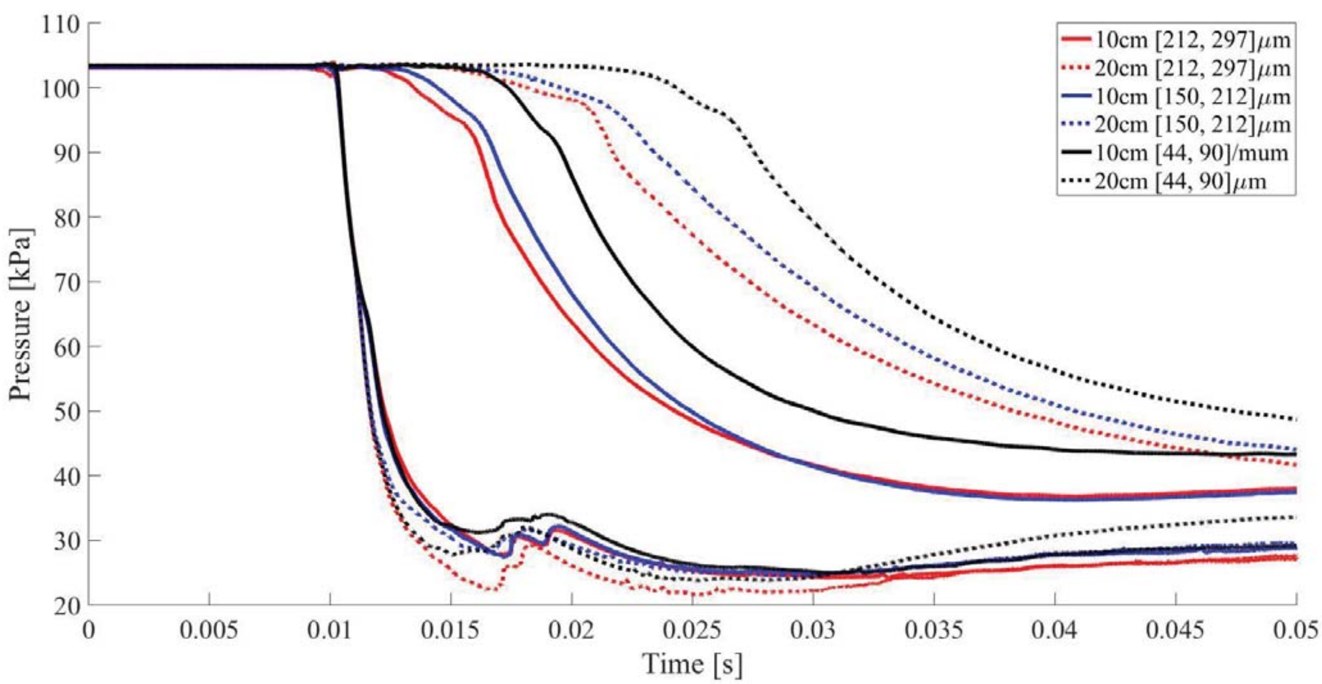

Summary of Bed Height and Pressure Data

- Bed height
  - Beds composed of smaller particles rise more quickly
  - Taller beds rise more quickly
    - This effect is magnified as particle diameter is increased
- Pressure
  - The rarefaction wave travels more slowly through beds composed of smaller particles
    - This effect is magnified as initial bed height is increased
  - The pressure above the particle bed interface drops more rapidly when the particle bed interface is closer to the diaphragm (*i.e.* the bed is taller)

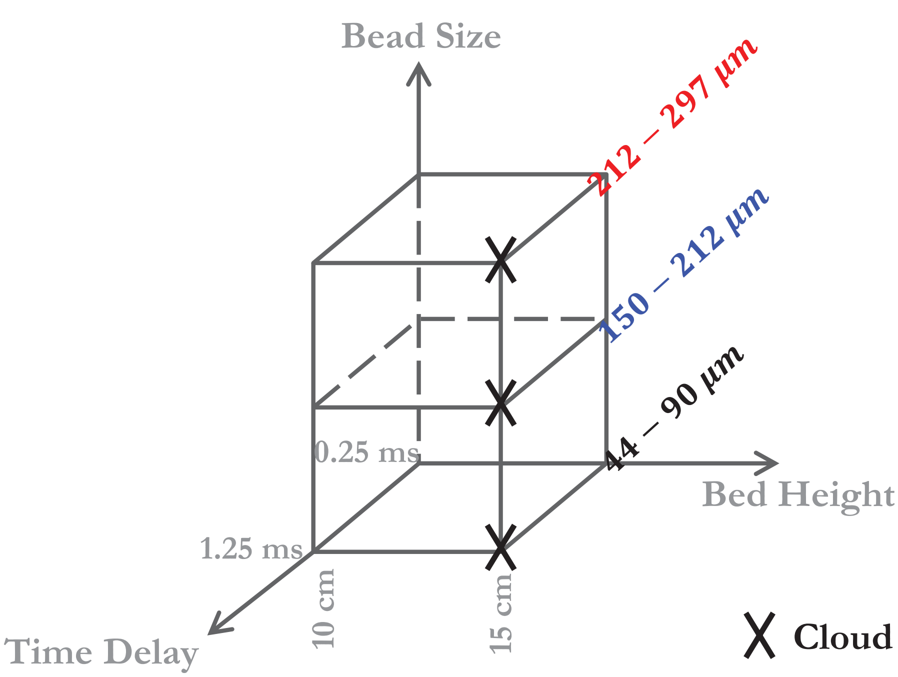

Results

- Effect of particle size in 10cm bed on gas velocity (short delay)

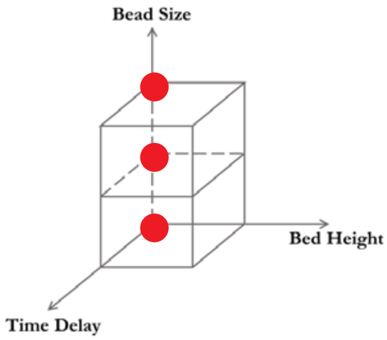

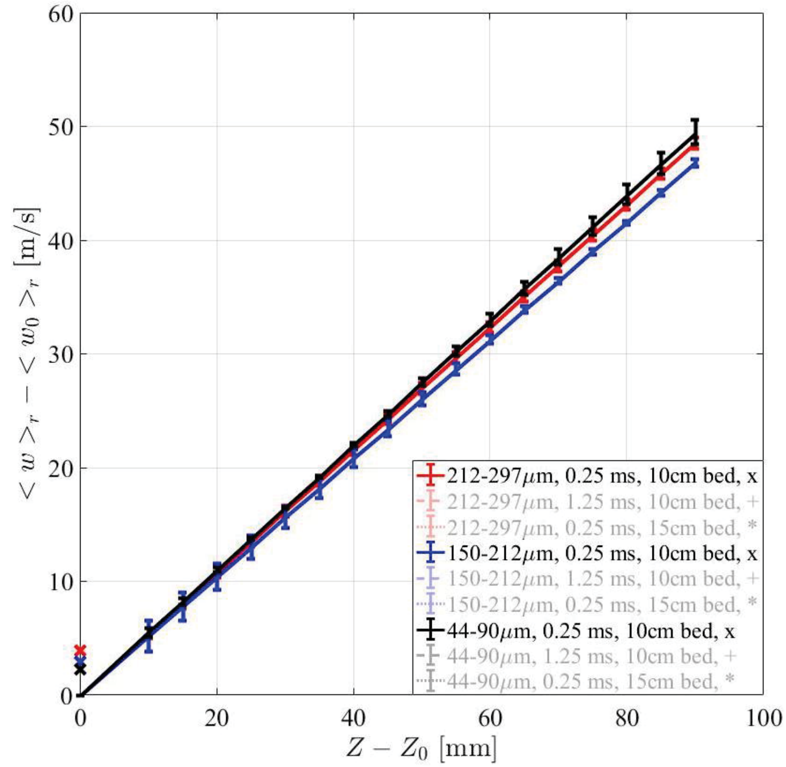

Results

- Effect of particle size in 10cm bed on gas velocity (long delay)

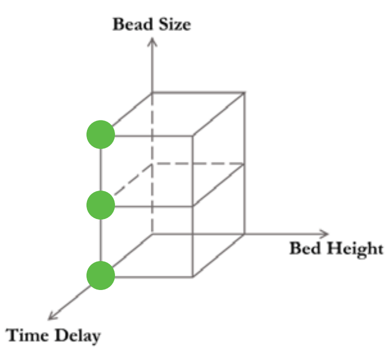

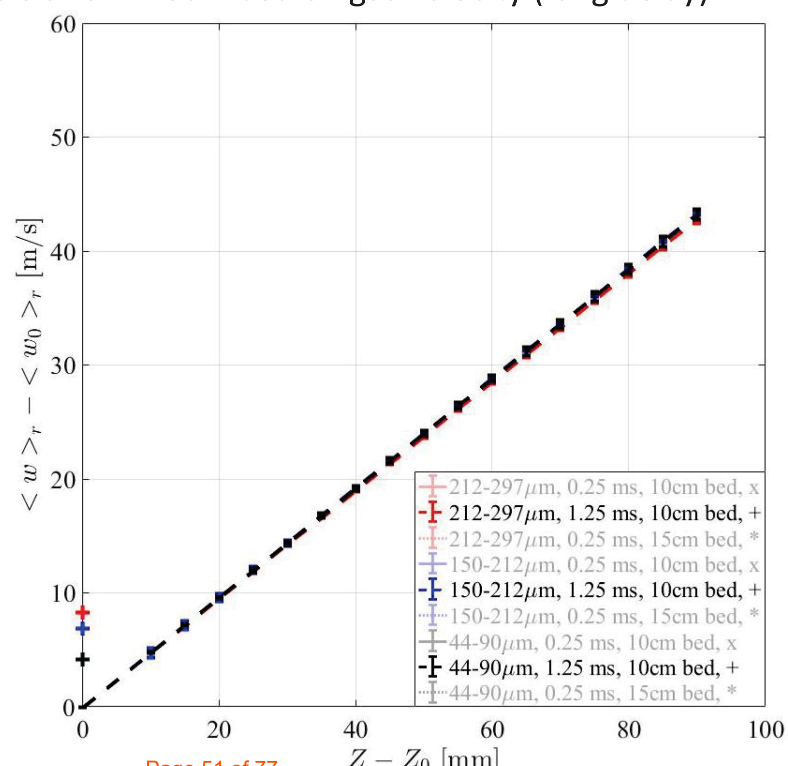

UF UNIVERSITY of FLORIDA

Results

- Effect of particle size in 15cm bed on gas velocity (short delay)

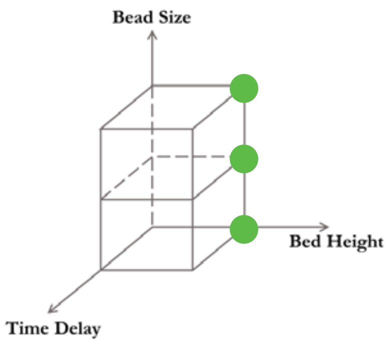

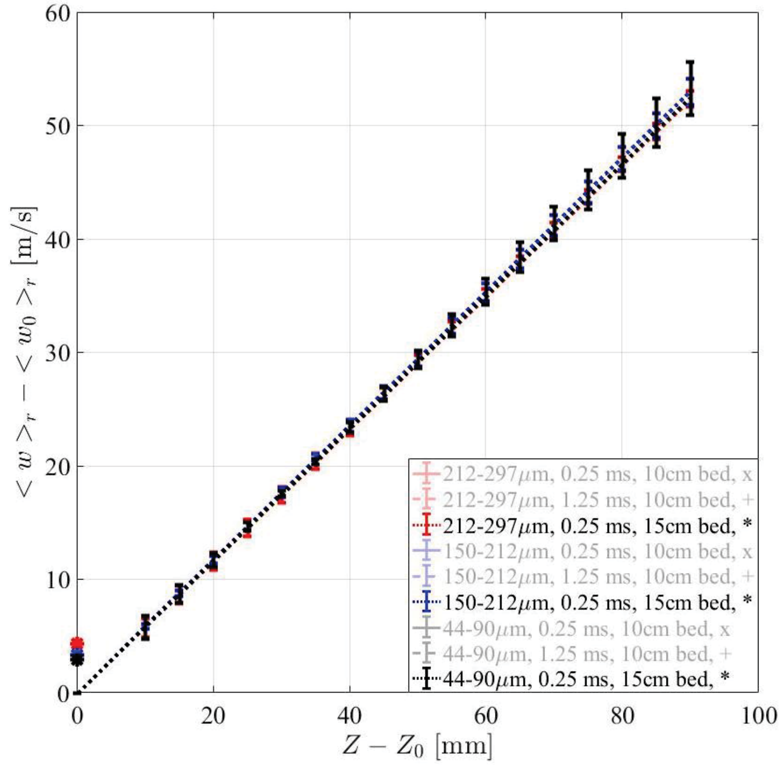

CCMT

UF UNIVERSITY of FLORIDA

Results

- Effect of time delay for [212, 297]µm

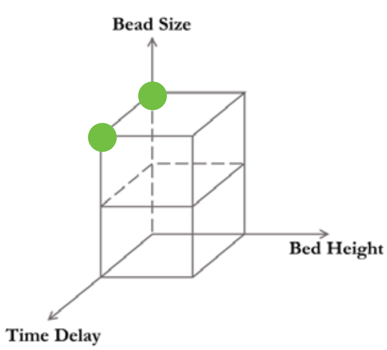

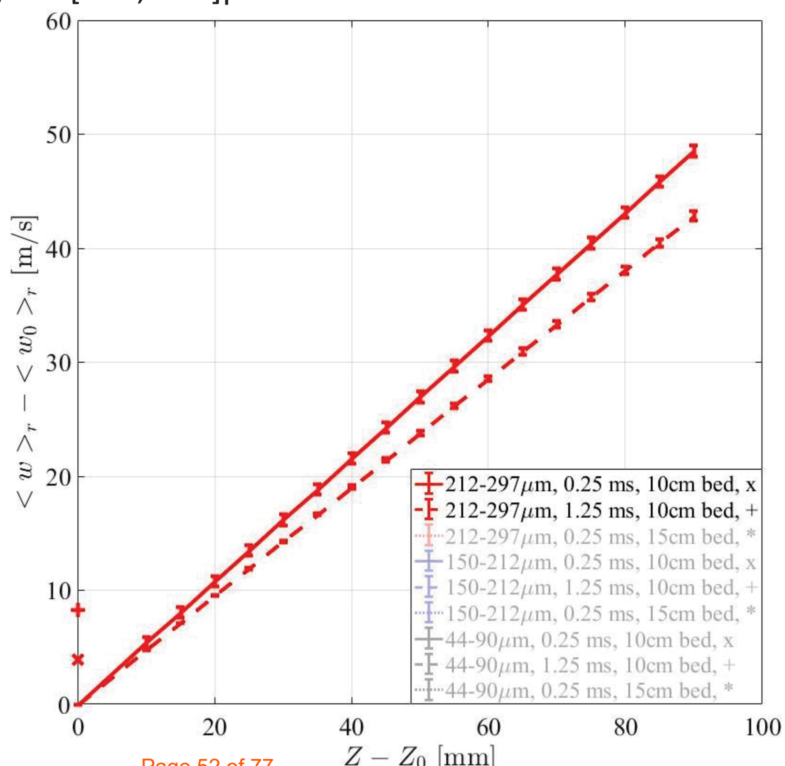

CCMT

UF | UNIVERSITY of FLORIDA

Results

- Effect of initial bed height at short time delay for [212, 297]µm

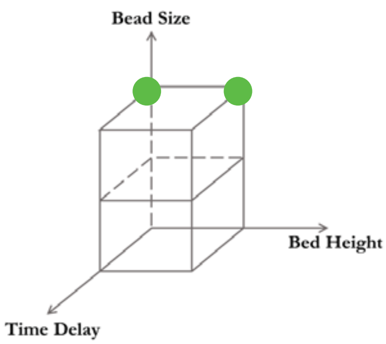

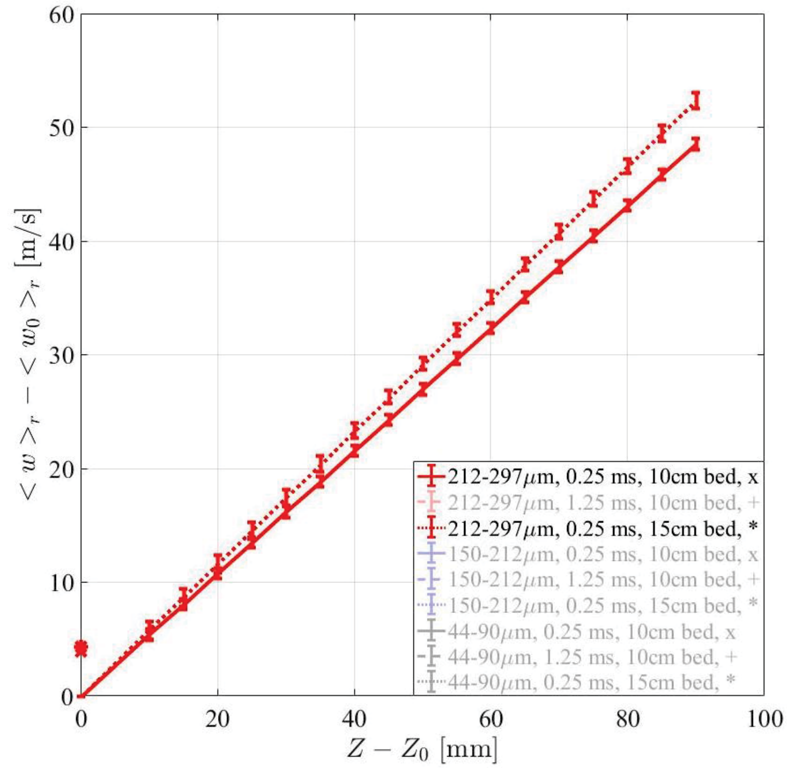

CCMT

UF | UNIVERSITY of FLORIDA

Results

- Effect of time delay for [150, 212]µm

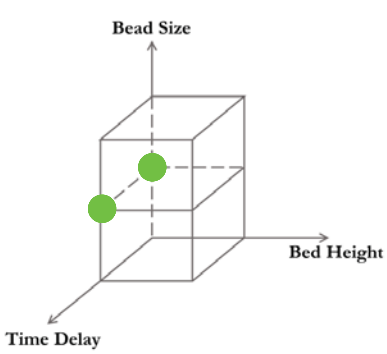

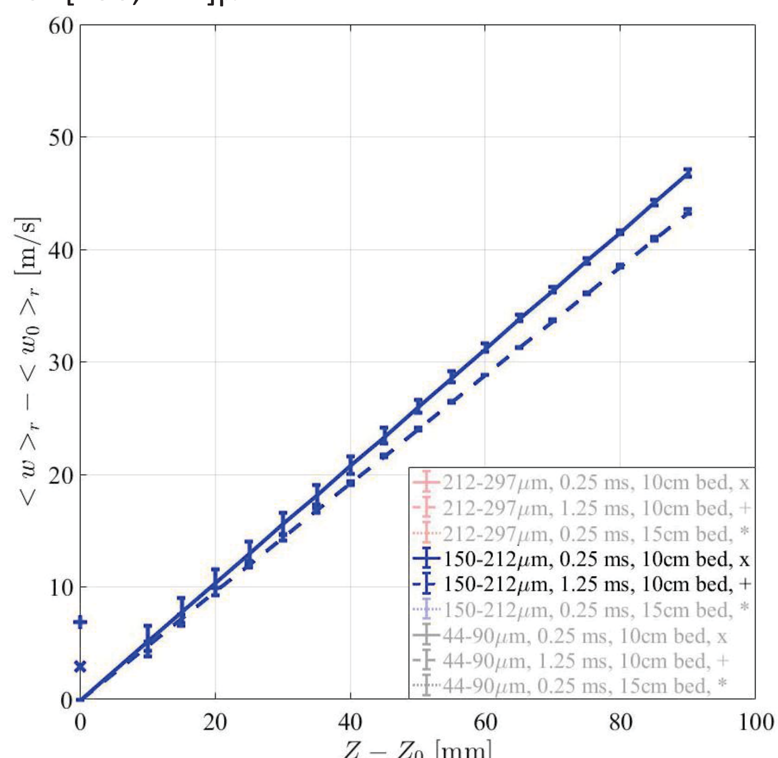

CCMT

Results

- Effect of initial bed height at short time delay for [150, 212]µm

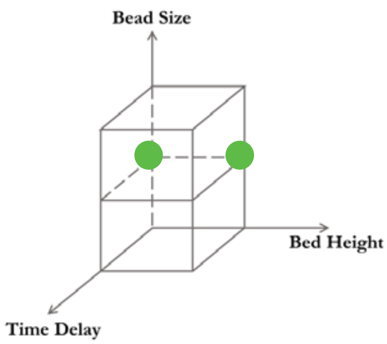

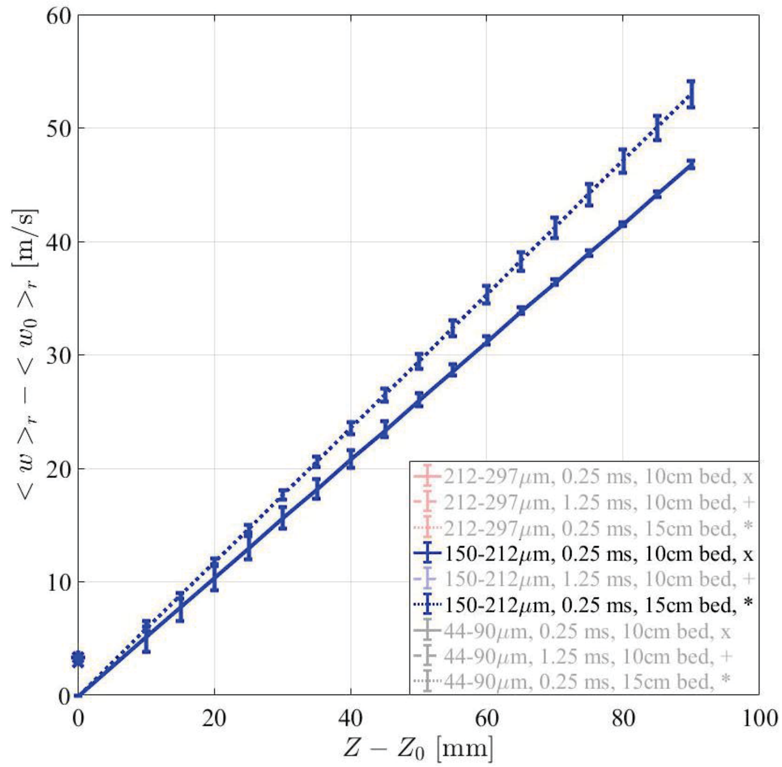

Results

- Effect of time delay for [44, 90]µm

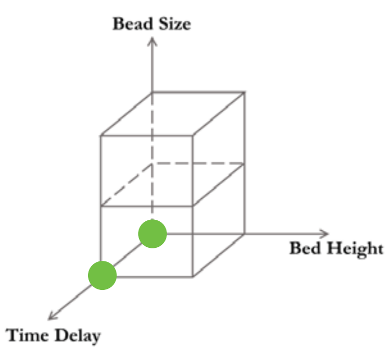

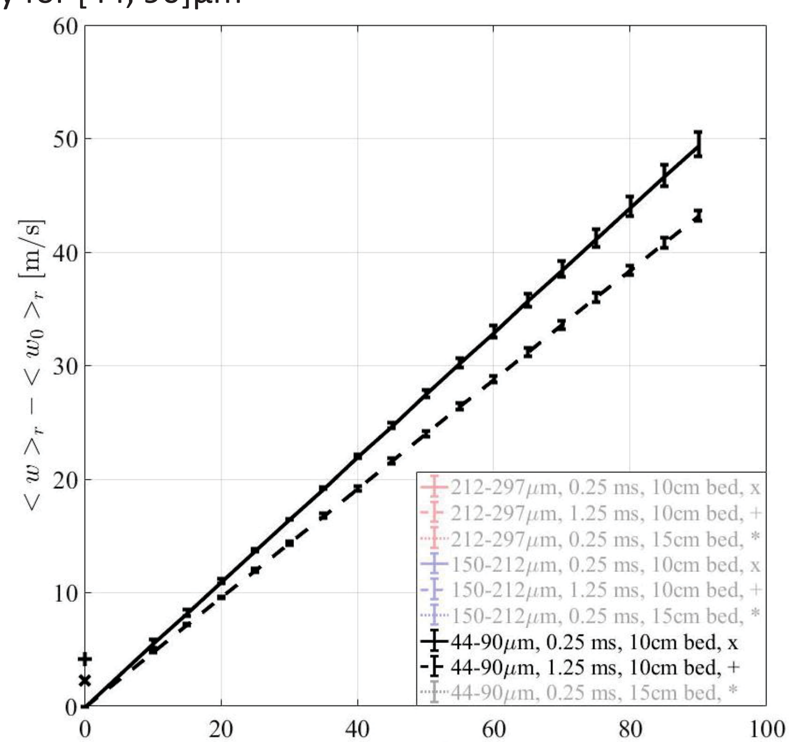

Results

- Effect of initial bed height at short time delay for [44, 90]μm

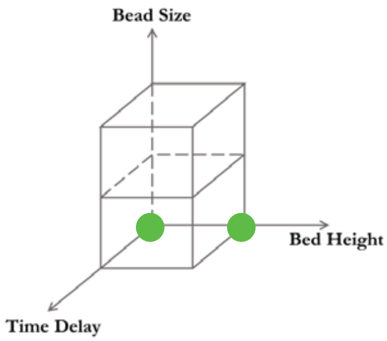

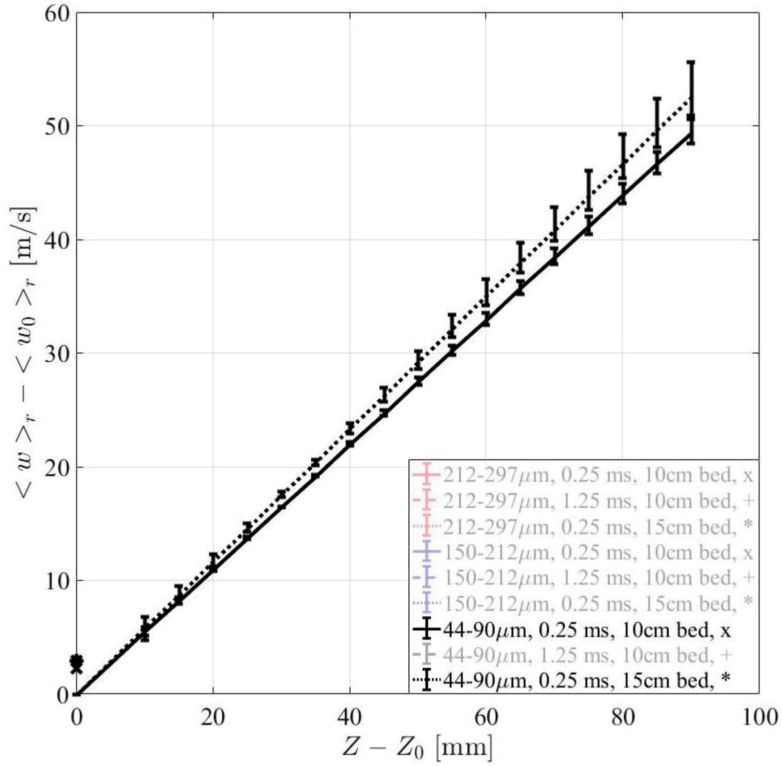

Summary of PIV Data

- Larger bead diameter yields higher gas velocity
  - Larger interstices and channels
  - Less impedance
- Taller initial bed height leads to higher gas velocity and stronger dilation
  - Pressure drop
- Gas dilation is more significant at earlier times
  - Velocity gradient

Do you have any questions?

CCMT

Dynamic load balancing techniques in CMT-nek

Keke Zhai
Computer and Information Science and Engineering
University of Florida

UF UNIVERSITY of FLORIDA

NNSA

UF UNIVERSITY of FLORIDA

Dynamic Load Balancing: Expansion Fan

CMT-nek Simulation

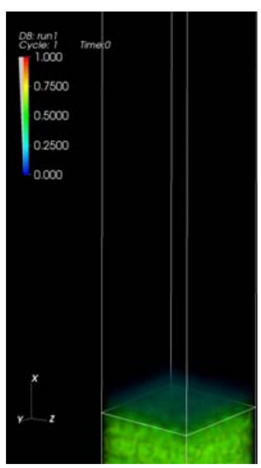

ASU Experiment

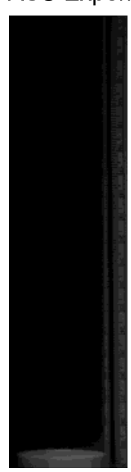

CCMT

2

Overview of Dynamic Load Balancing

- Step 1: Domain decomposition
  - Happens during initialization only
- Step 2: Elements to processor mapping
  - Happens during initialization and on every remapping
- Step 3: Decide when to trigger a remap
  - Rebalance after every k time steps (user set up)
  - Rebalance automatically after certain time steps (adaptive load balancing)
- Step 4: Transfer elements and particles and reset other data structures

CCMT

3

Overview of Dynamic Load Balancing

- Step 1: Multi-dimension to one-dimension conversion
  - Happens during initialization only
- Step 2: **Elements to processor mapping**
  - Happens during initialization and on every remapping
- Step 3: Decide when to trigger a remap
  - Rebalance after every k time steps (user set up)
  - Rebalance automatically after certain time steps (**adaptive load balancing**)
- Step 4: Transfer elements and particles and reset other data structures

CCMT

4

Overview of Element to Processor Mapping Algorithm

- Centralized
  - Easy to accomplish
  - There is a bottleneck where only processor P0 is working
  - Have more information to achieve better decision
- Distributed
  - There is no bottlenek at all
  - Each processor communicate with each other to get part information
  - Use limited information to make decision
  - MPI_allgatherv is taking most of the time on Quartz
- Hybrid
  - Combination of centralized and distributed
  - Utilize broadcast in replace of MPI_allgatherv to reduce communication time

Centralized Algorithm - Initial

Initially, each processor has an element load array

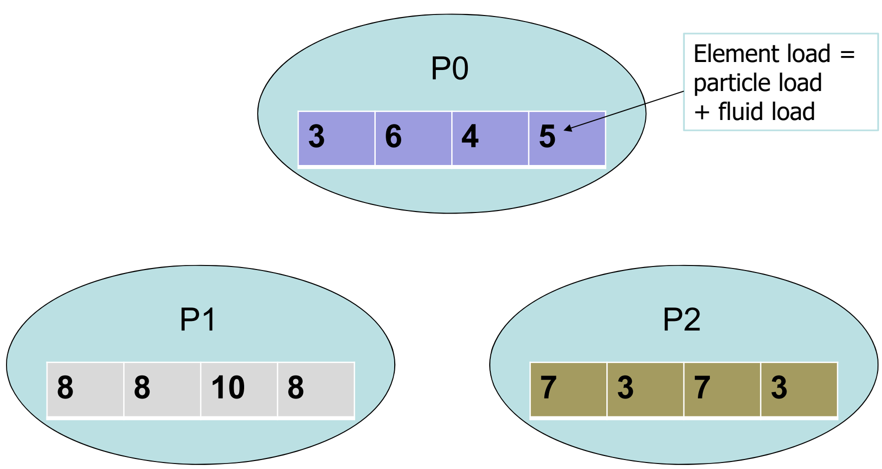

Centralized Algorithm - Send to P0

Each processor sends element load array to P0

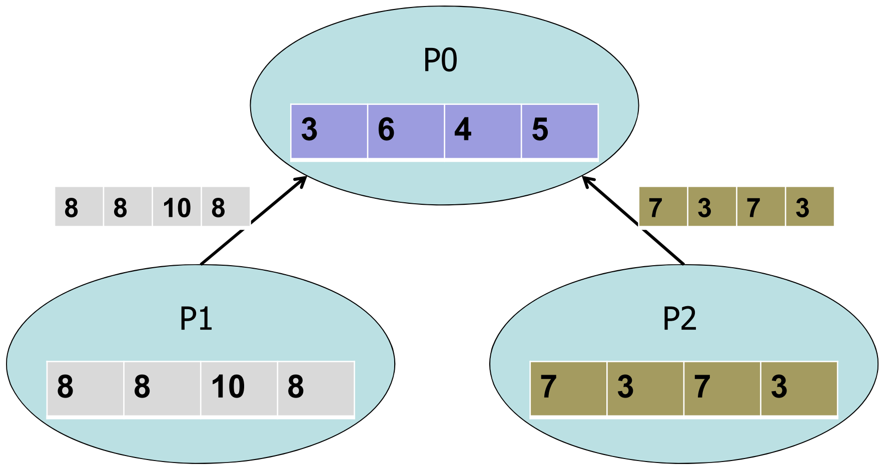

CCMT

7

Centralized Algorithm - Calculate Prefix Sum

P0 receives and concatenates the element load array, computes the prefix sum, divides prefix sum by average load

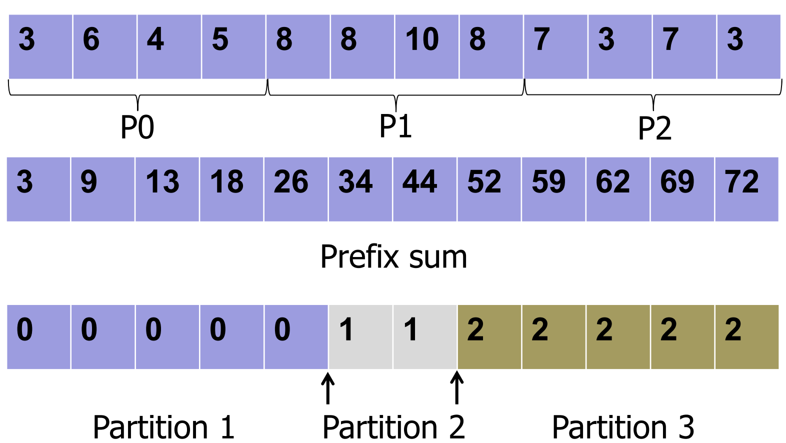

CCMT

8

Centralized Algorithm - Distribute Elements

P0 distributes the assignment to other processors, and each processor gets the new elements

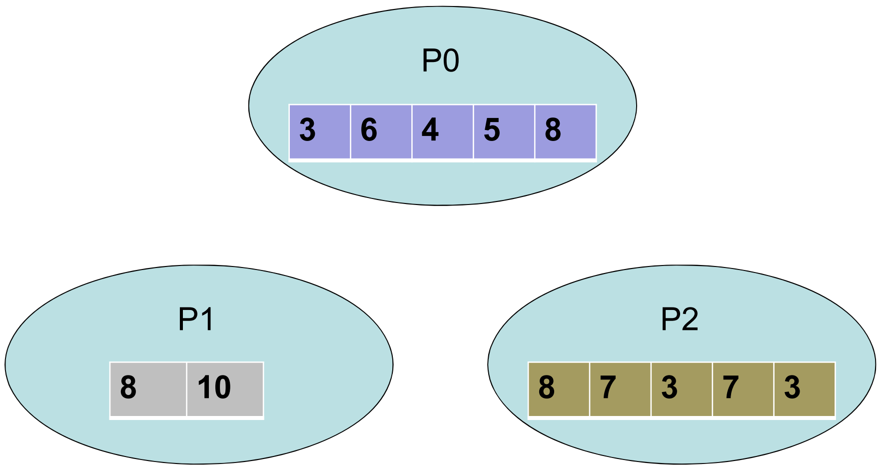

CCMT 9

Distributed Algorithm - Local Prefix Sum

Each processor computes local prefix sum and the exclusive prefix sum of the element load on each processor

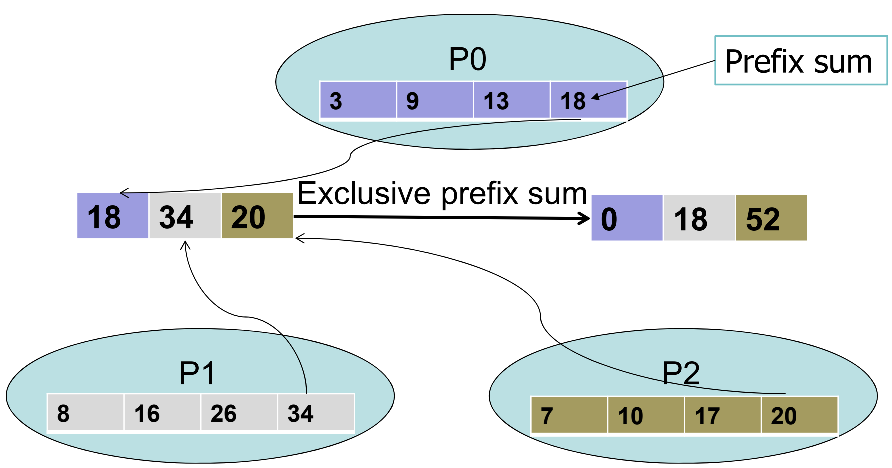

CCMT 10

UF UNIVERSITY of FLORIDA

Distributed Algorithm - Global Prefix Sum

Each processor adds the exclusive prefix sum to local prefix sum array to get the global prefix sum of element load array

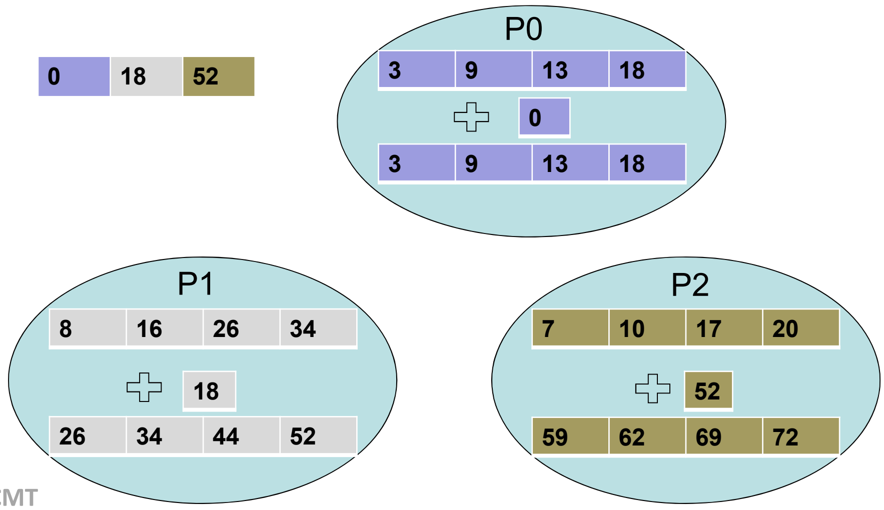

CCMT

11

UF UNIVERSITY of FLORIDA

Distributed Algorithm - Get Mapping

Each processor divides the global prefix array with the average load (in this case 24)

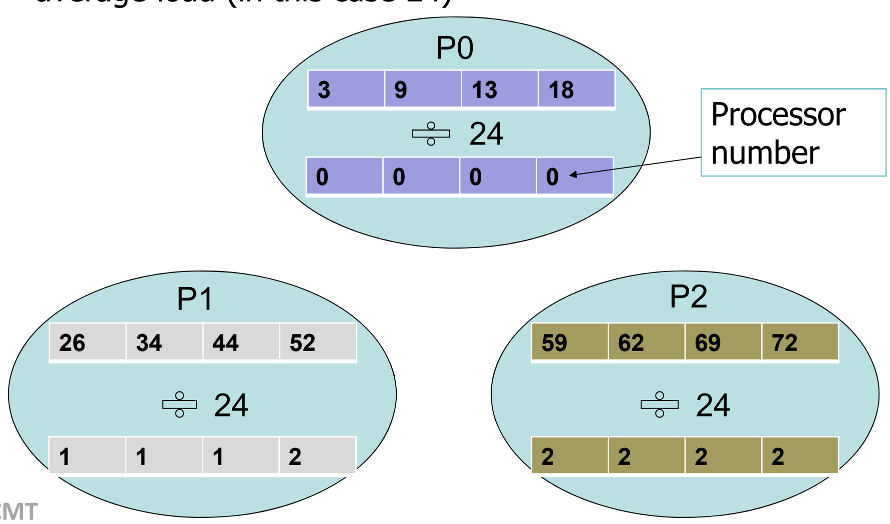

CCMT

12

Distributed Algorithm - Compressed Mapping

Each processor calls MPI_allgatherv to gather the element-> processor mapping.

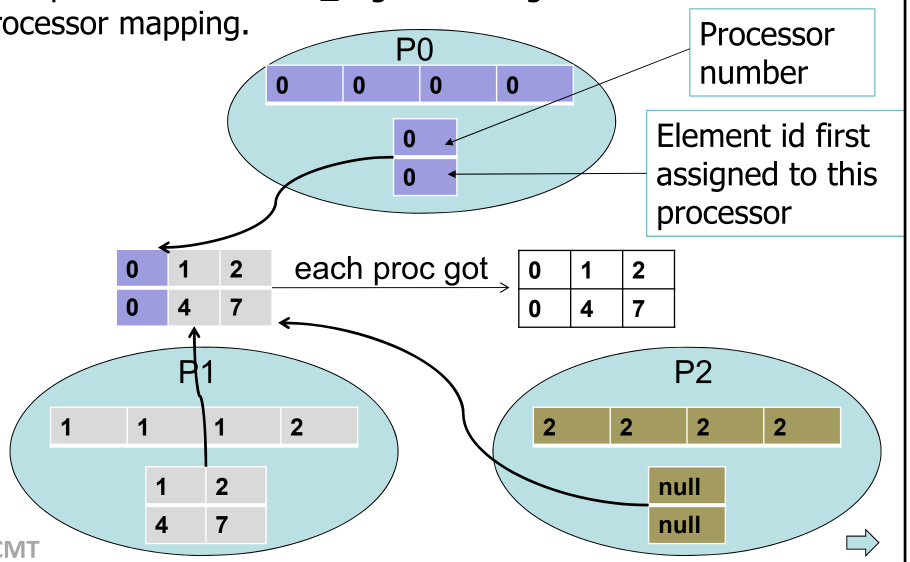

CCMT

13

Distributed Algorithm - Adjust Mapping

According to the element->processors mapping, each processor adjusts the mapping such that the number of elements in a processor exceed "*lelt*" (the maximum allowed). In this case, there is no need to adjust.

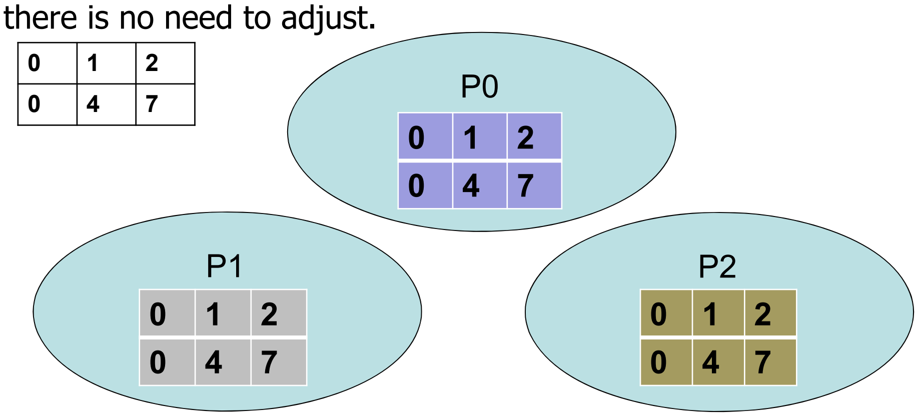

CCMT

14

Hybrid Algorithm - Send Compressed Mapping

The hybrid algorithm is similar to the distributed algorithm except for the step that get the global element->processor mapping. Each processor sends the mapping to P0.

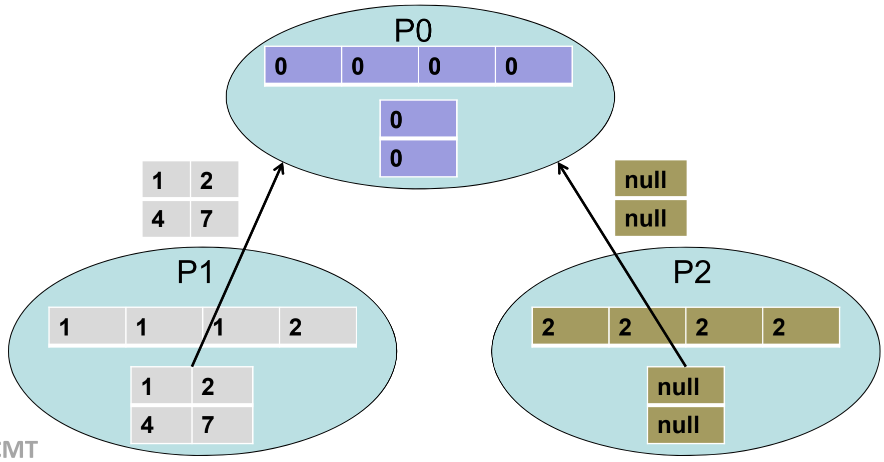

CCMT 15

Hybrid Algorithm - Distribute Elements

According to the element->processors mapping, processor P0 adjusts the mapping such that the number of elements in a processor exceed "*lelt*" (the maximum allowed). Then it broadcasts the result mapping to all processors.

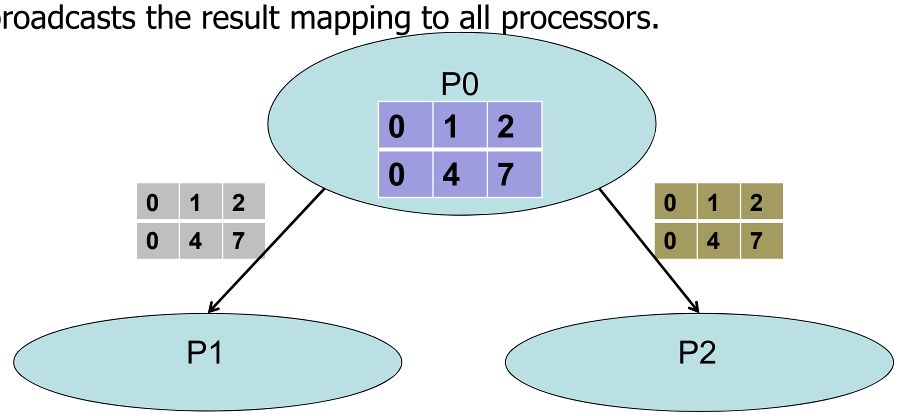

Dynamic Load Balancing for Compressible Multiphase Turbulence, Keke Zhai, Tania Banerjee, David Zwick, Jason Hackl and Sanjay Ranka, submitted to ICS 2018

CCMT 16

Adaptive Load Balancing Algorithm

- c1—— step right after first load balancing
- c2—— step right before second load balancing
- t1——time taken by step c1
- t2——time taken by step c2

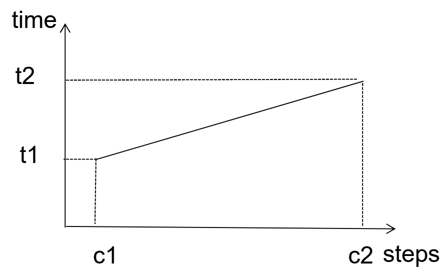

- lb_time——time taken for load balancing
- adaptiveLBInterval = $\sqrt{\frac{2*(c2-c1)*lb\_time}{t2-t1}}$ [1]
- adaptiveLBInterval: gives the next time step after c2 when load balancing should happen

[1] Menon H, Jain N, Zheng G, et al. Automated load balancing invocation based on application characteristics[C]//Cluster Computing (CLUSTER), 2012 IEEE International Conference on. IEEE, 2012: 373-381.

CCMT 17

Expansion testcase: CMT-nek on Quartz

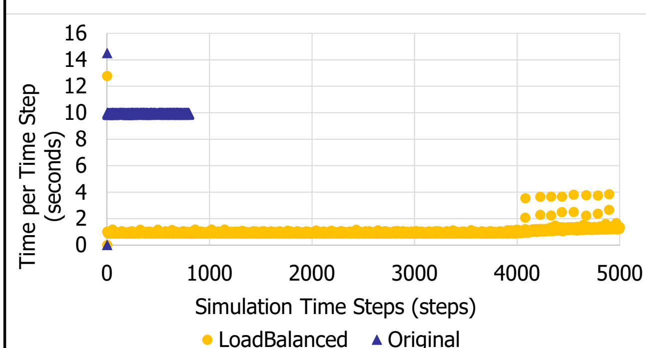

CMT-nek

67,206 MPI ranks
1,867 nodes
36 cores per node
900,000 elements
1,125,000,000 particles
Grid size: 5x5x5
Rarefaction test
9.97x improvement in performance

- Time per time step:
  - 9.92 s for the original code
  - 0.995 s for the load balanced code
- Adaptive hybrid load balancing were used and it first happened at 4077 time step.

CCMT 18

Expansion testcase: CMT-nek on Vulcan

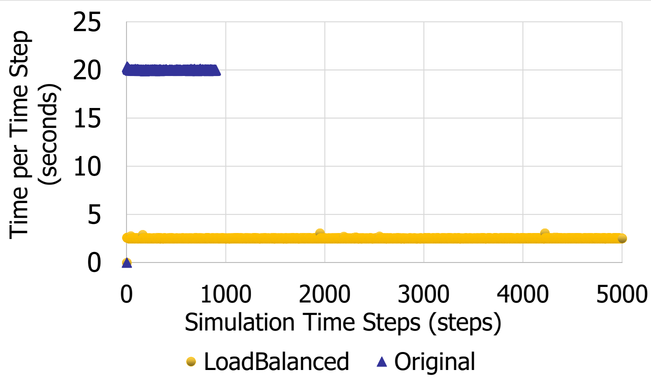

CMT-nek

65,536 MPI ranks
16,384 nodes
4 cores per node
900,000 elements
1,125,000,000 particles
Grid size: 5x5x5
Rarefaction test
7.9x improvement in performance

- Time per time step:
  - 20.00 s for the original code
  - 2.52 s for adaptive distributed load balanced code
- There was no need to load balance during the simulation since the time per time step didn't increase over the threshold set to trigger load balancing.

CCMT

19

Expansion testcase: Adaptive Load Balancing

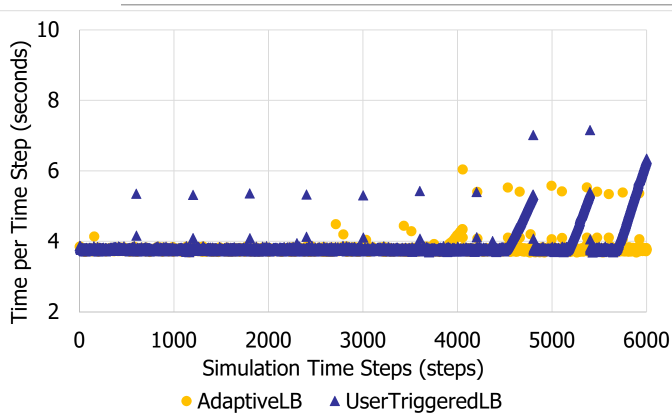

CMT-nek

32,768 MPI ranks
8,192 nodes
4 cores per node
460,800 elements
576,000,000 particles
Grid size: 5x5x5
Rarefaction test

- User-triggered load balancing algorithm: load balance every 500 time steps.
- Adaptive load balancing algorithm: first load balance after 4000 time step.
- Time per time step from step 4,000 to 6,000 for adaptive and user-triggered load-balancing algorithms was 3.78 s and 4.17 s, respectively.
- Giving us an overall improvement of 9.4%.

CCMT

20

CCMT

Do you have any questions?

UF UNIVERSITY of FLORIDA

NNSA

UF UNIVERSITY of FLORIDA

Rebalancing Time: Total Overhead (Quartz)

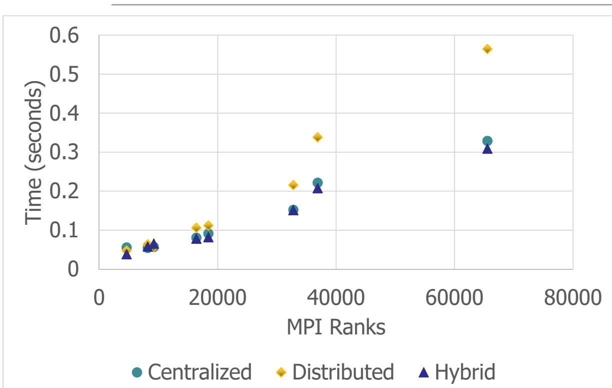

CMT-nek

Max: 65,520 MPI ranks
4 elements / rank
343 particles / element
Grid size: 5x5x5
Rarefaction test

- Overhead expressed as number of time steps:
  - 1.94 for the centralized
  - 3.35 for the distributed
  - 1.82 for the hybrid algorithm
- This shows that the overhead for load balancing is very small.

CCMT

22

UF UNIVERSITY of FLORIDA

Rebalancing Time: Total Overhead Time (Vulcan)

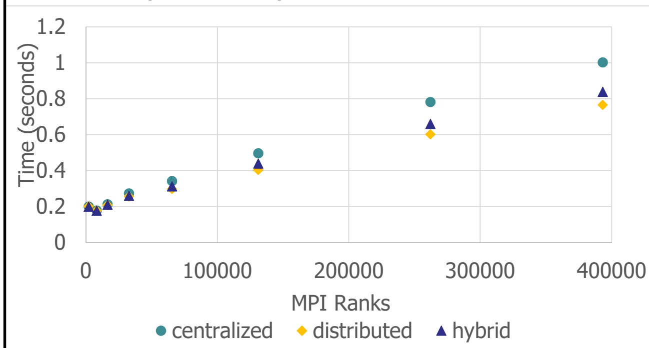

CMT-nek

Max: 393,216 processors
2 elements / rank
343 particles / element
Grid size: 5x5x5
Rarefaction test

- Overhead expressed as number of time steps:
  - 1.00 for the centralized
  - 0.77 for the distributed,
  - 0.84 for the hybrid algorithm

CCMT

23

UF UNIVERSITY of FLORIDA

Expansion testcase: Power consumption on Quartz (using Libmsr)

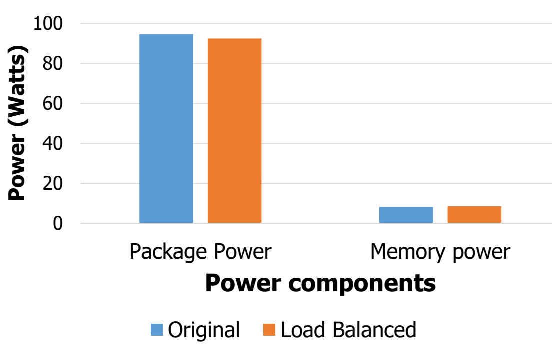

CMT-nek

67,206 MPI ranks
1,867 nodes
36 cores per node
900,000 elements
1.125×10^{9} particles
Grid size: 5x5x5
Rarefaction test
8.3x improvement in performance

- Power consumption is comparable.

CCMT

24

Expansion testcase: Power consumption on Mira (Using MonEQ)

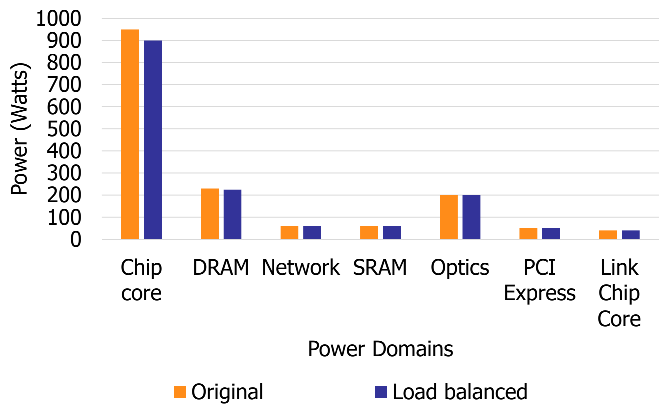

CMT-nek

4,608 processors
73,728 elements
86,400,000 particles
Grid size: 5x5x5
Rarefaction test
2x improvement in performance

- Core power and DRAM power reduced by about 5% and 2% respectively, leading to an overall reduction of 3.5% of total power when load balancing is used
- Energy consumption of the load balanced code is better because of reduced time as well as reduced power consumption

CCMT

25

CCMT

BE Simulations of CMT-nek:

Trace-driven simulation

Sai Chenna (BE)

BE Simulation of CMT-nek

CMT-nek BE-simulation

Normal Simulation:
- Workload is fixed
- Problem parameters (N,*nelt*,N_p): we either use a constant value or an approximate function
- Used for most DSE simulations

Trace-driven simulation:
- Workload is dynamic
- Uses a trace from specified problem to perform accurate simulations
- Used to perform DSE simulations for a specific problem

CCMT | 27

CMT-nek: Particle Solver subroutine

- **Particle solver** – *expensive kernel in CMT-nek*
  - Calculates the particle properties at each time-step
  - Assumptions :
    - No particle to particle interaction
    - No two-way coupling
  - Parameters:
    - *N – element size*
    - *nelt – elements-per-processor*
    - *α – particles/gridpoint*
    - N_p *- # particles =* $\alpha * N^3 * nelt$

CMT-nek Workflow

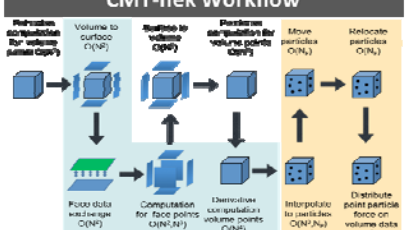

update_particle_location	Check if particle moved outside the box and update its location
move_particles_inproc	Move particles to processor which owns it
interp_props_part_location	Interpolate fluid properties at particle location
usr_particles_forces	Calculate fluid forces acting on the particle
update_vel_and_pos	Update particle position and velocity

CCMT | 28

Trace-driven simulation: Particle-solver

- CMT-nek Particle solver:
  - Workload per processor depends on # particles
  - # particles/processor is dynamic:
    - varies among processors – *depends on problem and mapping algorithm*
    - varies at each timestep – *based on fluid forces on particles*
  - Need a trace to perform simulations

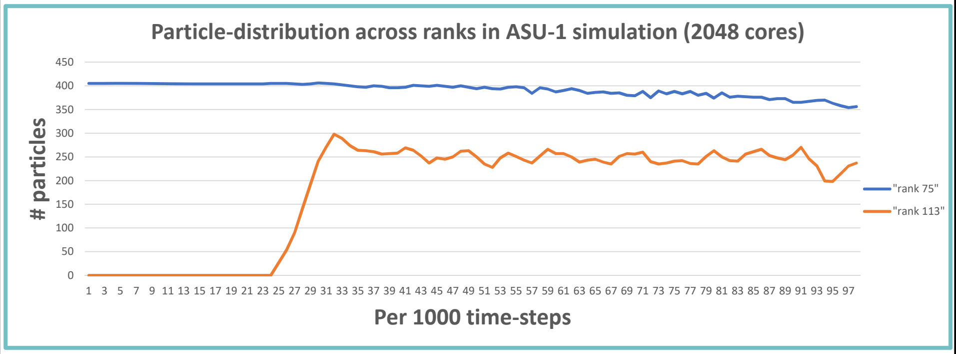

CCMT

29

Modelling Approach: Trace-driven simulation

- Particle-workload distribution tool:
  - **Key principle**: Particle movement doesn't depend on processor count
    - Single trace for a given problem size is sufficient to predict particle movement for any # of processors
  - Input:
    - trace data containing particle and element mapping at each time-step
    - No of ranks we want to simulate
    - Mapping algorithm
  - Output:
    - # particles residing in each rank @ every timestep – ***computation workload***
    - # particles moving across each rank @ every timestep – ***communication workload***

0	1
2	3

0	1	2	3
4	5	6	7
8	9	10	11
12	13	14	15

CCMT

30

Case study : ASU-1

- Experimental Setup:
  - Problem: ASU-1
  - # of Particles: 133341
  - # of elements: 15768
  - Element size: 4
  - Particle trace frequency: 1000 time-steps

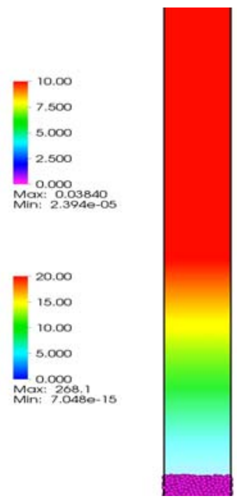

CCMT

31

Particle-workload distribution tool: ASU-1

ASU-1 particle-workload distribution on 256 cores (Vulcan)

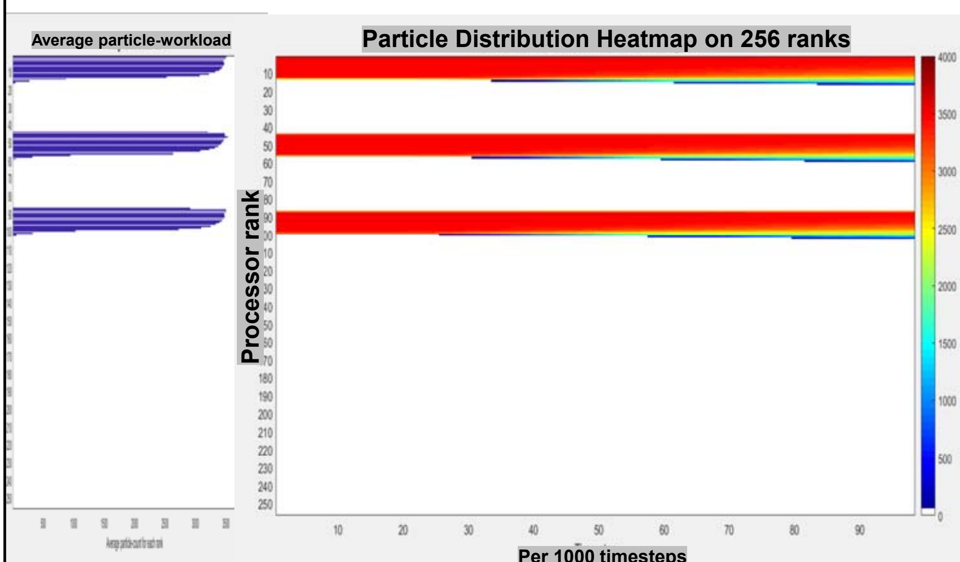

32

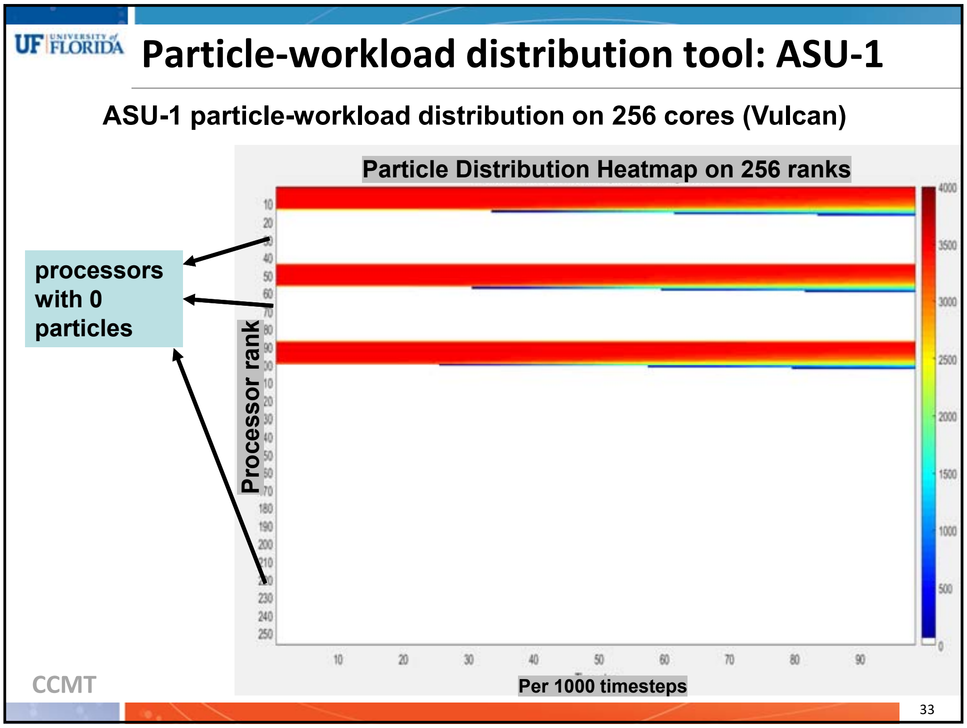
Particle-workload distribution tool: ASU-1
ASU-1 particle-workload distribution on 256 cores (Vulcan)
Particle Distribution Heatmap on 256 ranks
processors with 0 particles
Processor rank
Per 1000 timesteps
CCMT
33

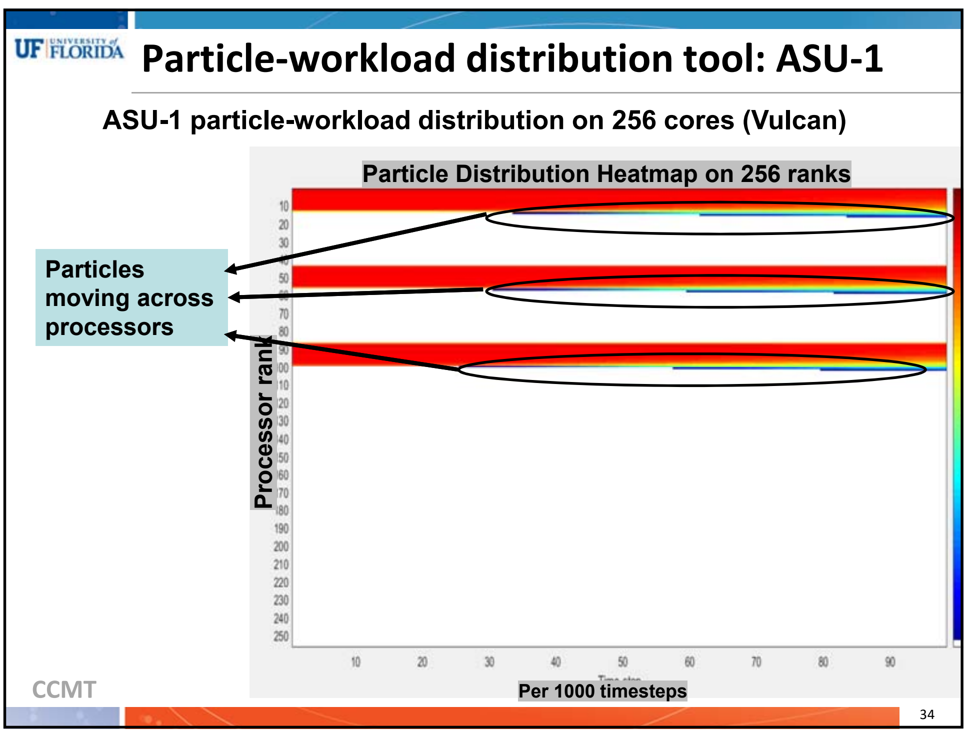
Particle-workload distribution tool: ASU-1
ASU-1 particle-workload distribution on 256 cores (Vulcan)
Particle Distribution Heatmap on 256 ranks
Particles moving across processors
Processor rank
Per 1000 timesteps
CCMT
34

Particle-workload distribution tool: ASU-1

ASU-1 particle-workload distribution on 4k cores (Vulcan)

Genmap – Recursive Bisection algorithm | **Load-balancing algorithm**

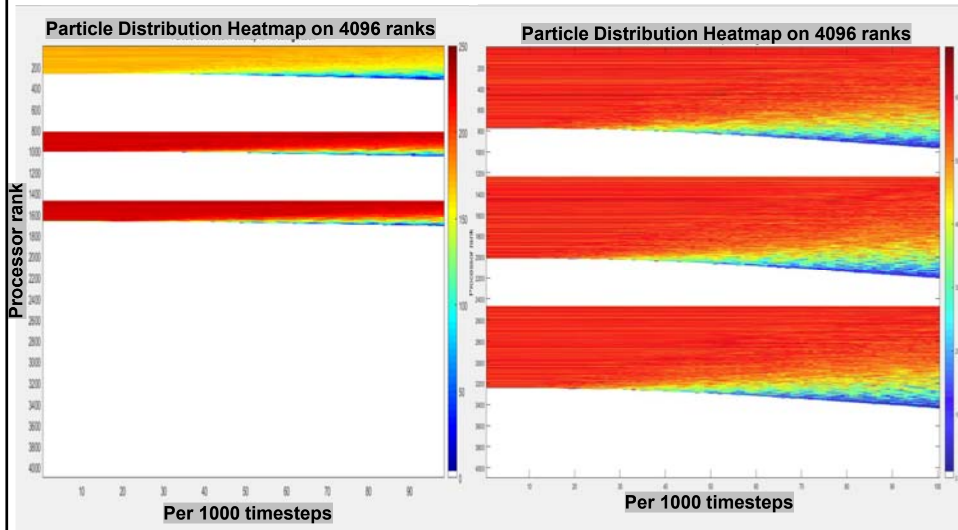

35

Particle-workload distribution tool: Results

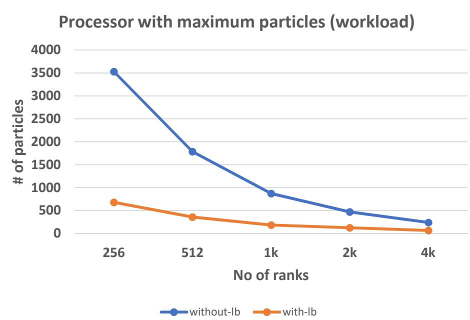

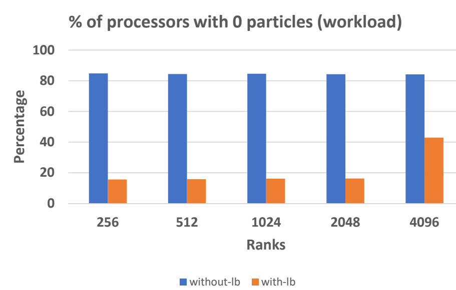

- Increase in processor-count results in:
  - *Reduced maximum particles-per-processor(workload)*
  - *Poor resource utilization*
  - *Increase in particle-communication*

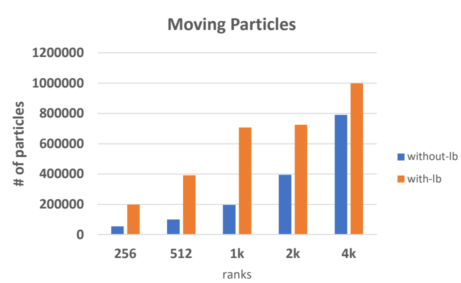

CCMT

36

UF UNIVERSITY of FLORIDA

Trace-driven simulation: Workflow

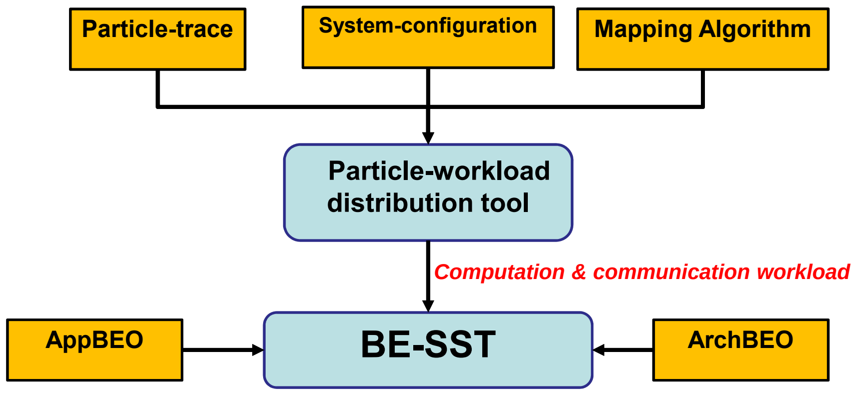

- Trace-driven simulation provides optimal configuration by identifying:
  - Computation cost
  - Communication cost
  - Resource utilization

CCMT

37

UF UNIVERSITY of FLORIDA

Conclusion

- Increase in processor-count results in:
  - ***Reduced*** *average particles-per-processor(workload)*
  - ***Poor*** *resource utilization*
  - ***Increase*** *in particle-communication*
- ***load-balancing algorithm*** can result in better resource utilization:
  - Particle-workload distribution tool can be helpful in determining the frequency of load-balancing to optimize the overhead
- Trace-driven simulation provides optimal configuration by identifying:
  - Computation cost
  - Communication cost
  - Resource utilization

CCMT

38

CCMT

Do you have any questions?

Particle-workload distribution tool: Results

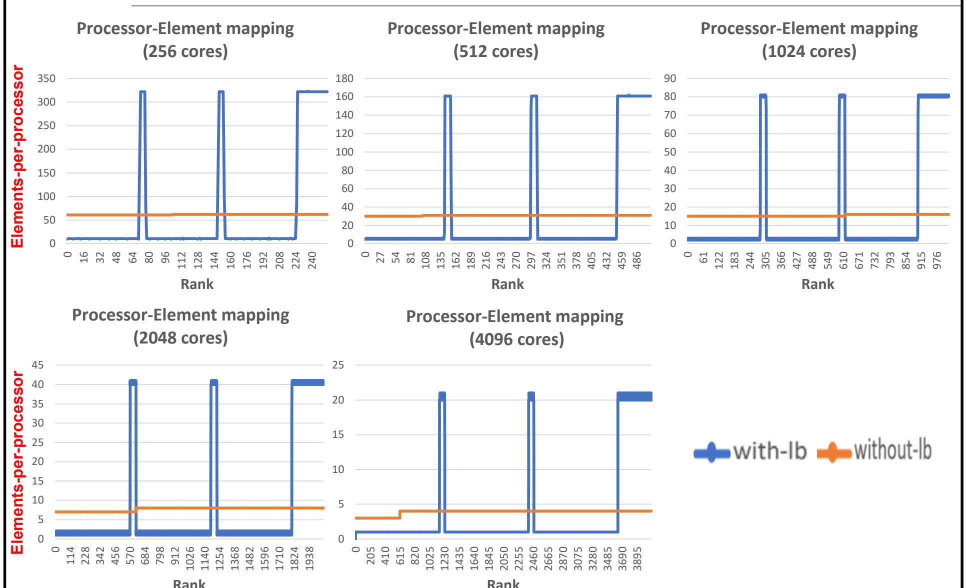

CCMT

40

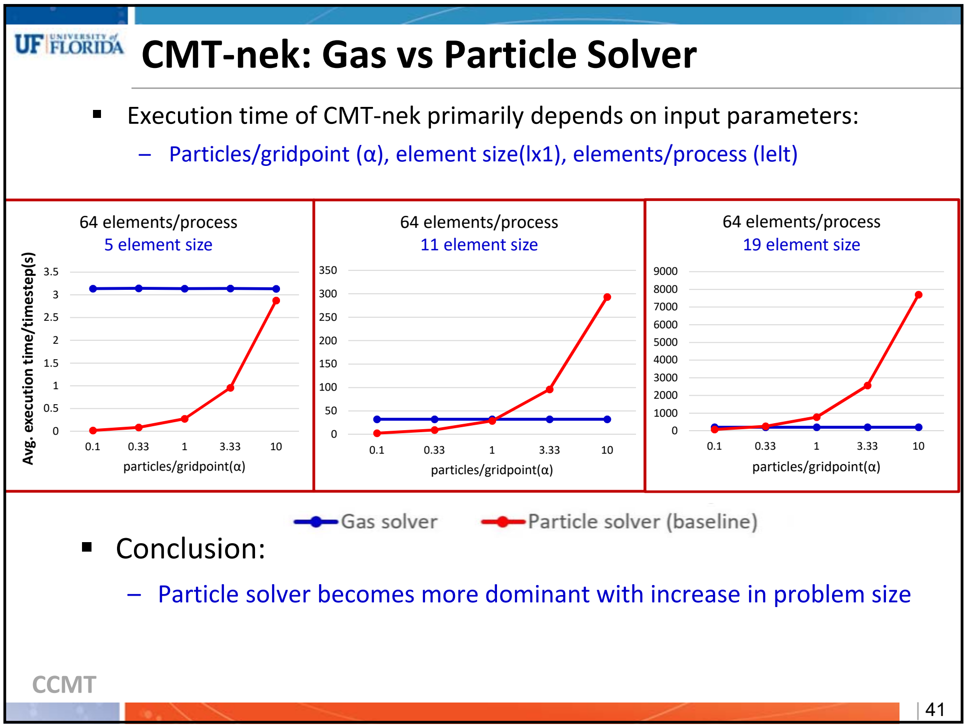
UF FLORIDA
CMT-nek: Gas vs Particle Solver
Execution time of CMT-nek primarily depends on input parameters:
– Particles/gridpoint (α), element size(lx1), elements/process (lelt)
64 elements/process
5 element size
Avg. execution time/timestep(s)
3.5
3
2.5
2
1.5
1
0.5
0
0.1
0.33
1
3.33
10
particles/gridpoint(α)
64 elements/process
11 element size
350
300
250
200
150
100
50
0
0.1
0.33
1
3.33
10
particles/gridpoint(α)
64 elements/process
19 element size
9000
8000
7000
6000
5000
4000
3000
2000
1000
0
0.1
0.33
1
3.33
10
particles/gridpoint(α)
Gas solver
Particle solver (baseline)
Conclusion:
– Particle solver becomes more dominant with increase in problem size
CCMT
| 41